Vrije Universiteit Brussel

Wavelet Transform

Course Notes

Jan Cornelis, Adrian Munteanu

ETRO Department
Vrije Universiteit Brussel

Contents of the Course[*]

[*]The first two sections discuss general DSP theory and are not presented in this document.

6. Wavelet Bases & Filter Banks

3. Time-Frequency Representations

3.1. Time- Frequency Representation

When calculating a signal expansion, a primary concern is the localization of a given basis function in time and in frequency. For example, in the Fourier transform, the functions used in the analysis of a given signal, are infinitely sharp in their frequency localization (they exist at one precise frequency) but have no time localization because of their infinite extent. This means that the transients in the signal are not captured accurately with a Fourier analysis. Practical applications aim at “localizing” the analysis of the signal, therefore basic modifications are required to improve the "time localization" properties of the basis functions. One way to define the localization of a particularly basis function is the "spread" in time and in frequency given by the intervals I_t and I_ω.

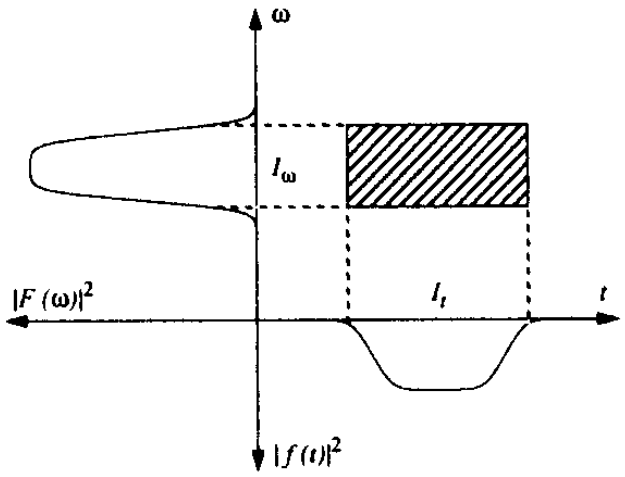

Figure 3.1.1. Tile in the time-frequency plane as an approximation of the time-frequency localization of $f(t)$.

These intervals contain 90% of the energy of the time and frequency-domain functions, and are centered around the centers of gravity of $|f(t)|^2$, respectively $|F(\omega)|^2$. This defines what is called a *tile* in the time- frequency domain.
We consider further elementary operations on a basis function $y(t)$ and their effects on the tile.
A shift in time by t results in shifting of the tile by t ; modulation by $e^{j\omega_0 t}$ shifts the tile in frequency by w_0. Finally, scaling by *s*, i.e. $f'(t) = f(st)$ results in $I'_t = I_t / s$ and $I'_w = sI_w$.
As we note, these elementary operations conserve the surface of the time-frequency tile. Remark that in the scaling case, resolution in frequency was traded for resolution in time.
In general, the *scaling* of a basis function $y(t)$ is defined as:

$$y_{a,b}(t) = \frac{1}{\sqrt{a}} y\left(\frac{t-b}{a}\right)$$

If the scaled basis function $y_{a,b}(t)$ is used to analyze a signal, the long term trends in the signal are captured for large values of *"a"*, while for small values, the short term behavior in the signal is followed.

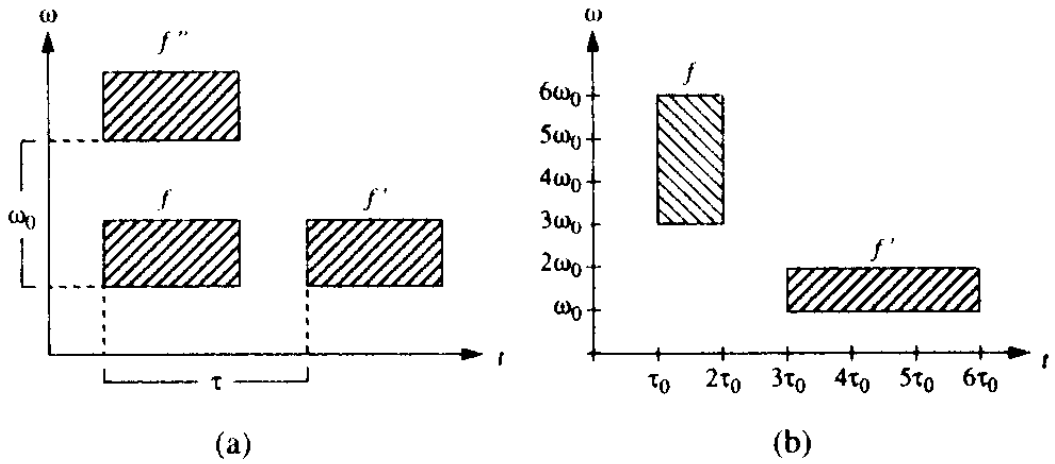

Figure 3.1.2. Elementary operations on a basis function f and effect on the time-frequency tile. (a) Shift in time by t producing f' and modulation by w_0 producing f''. (b) Scaling $f'(t) = f(st)$ ($s = 1/3$ is shown).

3.2. Uncertainty Principle

As indicated previously, there is a trade off between the resolution in frequency and the resolution in time and there is no way to get sharp analysis in both domains simultaneously. This is revealed by the uncertainty principle.

Consider a window function $g(t)$ with Fourier transform $G(w)$ centered around the origin in time and in frequency. Define the time width Δt of $g(t)$ by:

$$\Delta t^2 = \frac{\int t^2 |g(t)|^2 dt}{\int |g(t)|^2 dt},$$

and its frequency width Δw by"

$$\Delta w^2 = \frac{\int w^2 |G(w)|^2 dw}{\int |G(w)|^2 dw}.$$

If $g(t)$ vanishes faster than $1/\sqrt{t}$ as $t \to \infty$, then

$$\Delta t \cdot \Delta w \geq \frac{1}{2},$$

where the equality holds for Gaussian signals, $g(t) = \sqrt[4]{\frac{2a}{p}} e^{-a\,t^2}$

The uncertainty principle is fundamental since it sets a bound on the maximum joint sharpness or resolution in time and frequency of *any* linear transform. It is easy to check that scaling does not change the time-bandwidth product, it only exchanges one resolution for the other, similarly to what was shown in figure 3.1.2.

4. STFT, CWT and Frames Theory

4.1. Continuous Short-Time Fourier Transform

To improve the localization properties of the Fourier transform the windowed Fourier transform (or short time Fourier transform) was introduced. The signal is first multiplied by a window function $w(t-t)$ centered around the location of interest t and then the usual Fourier transform is taken. This leads to:

$$STFT_f(t,w) = \int_{-\infty}^{\infty} f(t)\cdot w^*(t-t)\cdot e^{-jwt}dt$$

This is equivalent with the inner product between the signal and the "shifts and modulates of the elementary window $w(t)$":

$STFT_f(\tau,\omega) = \langle f(t), g_{\omega,\tau}(t)\rangle$, where $g_{\omega,\tau}(t) = w(t-\tau)e^{j\omega t}$

It can be easily shown that the time-frequency resolution of each elementary function is constant, therefore it is natural to discretize the STFT on a rectangular grid $(m\omega_0, n\tau_0)$ (see figure 4.1.1 – (a) and (b)). More details concerning the discretization of the continuous STFT will be given in section 4.3.

The function $f(t)$ can be recovered in the L^2 sense ($L^2(R)$ is the vectorial space of square integrable functions) by a double integral:

$$f(t) = \frac{1}{2\pi\|w(t)\|^2}\int_{-\infty}^{\infty}\int_{-\infty}^{\infty} STFT_f(\omega,\tau)\cdot g_{\omega,\tau}(t)\,d\omega d\tau$$

The *spectogram* is defined as the energy distribution of the STFT:

$$S_f(\omega,\tau) = \left|STFT_f(\omega,\tau)\right|^2$$

Any classical window used for Fourier analysis is suitable for STFT transform. However, to have better frequency localization, smooth windows are preferred.
An example is the Hanning window, given by:

$$w(t) = \begin{cases}\left[1+cos(2\pi t/T)\right] & t\in[-T/2, T/2]\\ 0 & otherwise\end{cases}$$

The Gaussian window originally proposed by Gabor (yielding the so-called Gabor-analysis) is given by:

$w(t) = \beta e^{-\alpha t^2}$, $\alpha,\beta>0$, where α controls the width and β is a normalization factor.

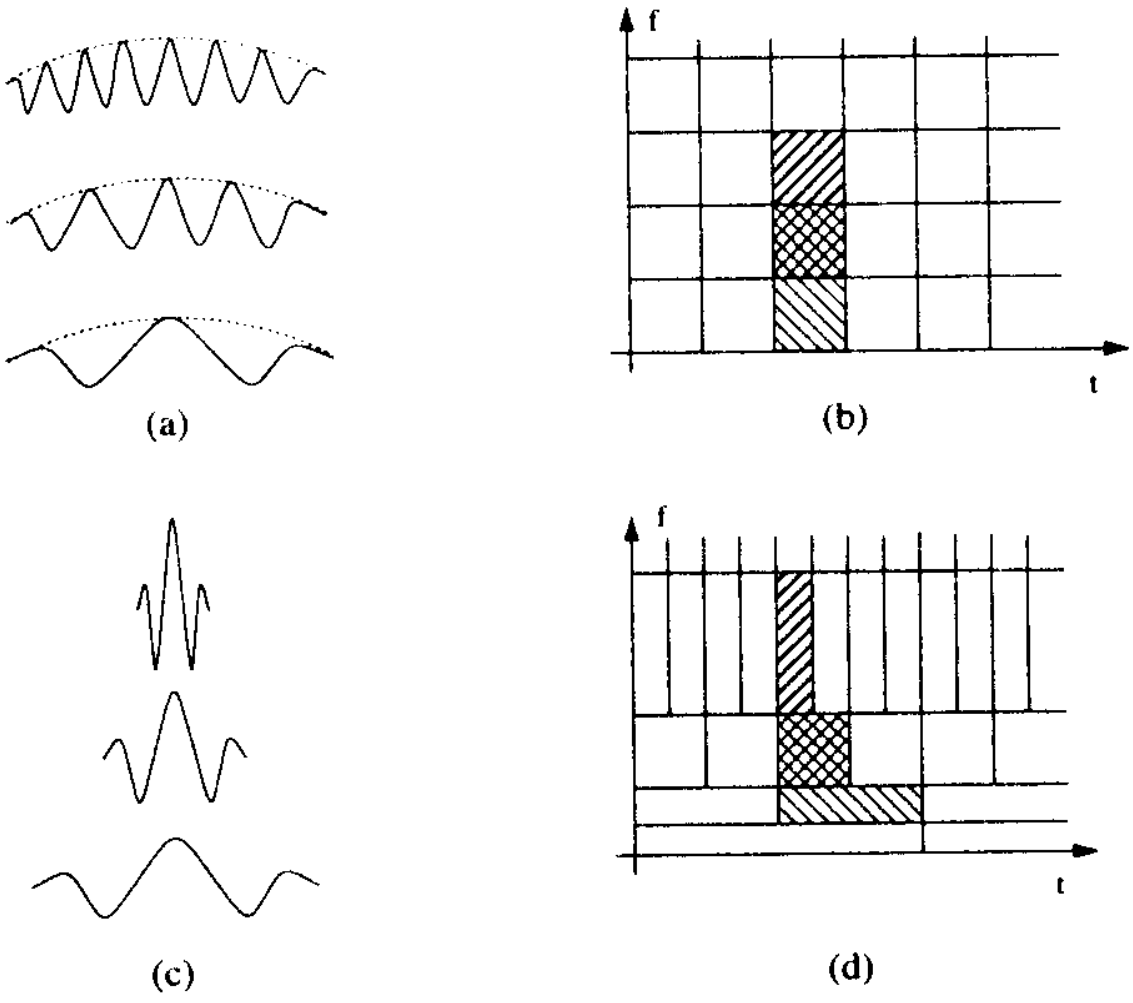

Figure 4.1.1. The short-time Fourier and wavelet transform. (a) Modulates and shifts of a Gaussian window used in the expansion. (b) Tiling of the time-frequency plane. (c) Shifts and scales of the prototype bandpass filter. (d) Tiling of the time-frequency plane.

4.2. Continuous Wavelet Transform.

The drawback introduced by the STFT is the constant resolution in time and frequency. Instead, we can use a constant relative bandwidth analysis and one can obtain changing time-frequency tiles due to the scaling. We impose:

$$\frac{\Delta f}{f} = c \,(\text{constant})$$

From the uncertainty principle, $\Delta t \cdot \Delta w \geq \frac{1}{2}$, therefore if equality is considered, we can write: $\Delta t = \frac{1}{2wc}$. From this expression we observe that the resolution in time is small at high frequencies and higher at the lower ones.

Consider a real band-pass filter with impulse response $y(t)$, zero mean $\int_{-\infty}^{\infty} y(t)dt = 0$, and unit energy; the continuous wavelet transform is defined as:

$$CWT_f(a,t) = \frac{1}{\sqrt{a}} \int_{-\infty}^{\infty} f(t) \cdot y^*\left(\frac{t-t}{a}\right) dt$$

If we write $y_{a,t}(t) = \frac{1}{\sqrt{a}} \cdot y\left(\frac{t-t}{a}\right)$ (see section 3.1), we deduce that the continuous wavelet transform measures the similarity between the signal and the scaled and shifted version of some elementary basis function $y(t)$:

$$CWT_f(a,t) = \left\langle f(t), y_{a,t}(t) \right\rangle$$

The discretization of the time-frequency space uses large time steps for large $a(a>1)$, and fine time steps for small *a*; the tiling of the time-frequency plane is given in figure 4.1.1 – (c) and (d). Since we are mostly interested to work with discrete signals and consequently with discrete transforms, we will give more details concerning the discretization of the continuous wavelet transform in section 4.3.

In order to be able to recover the original signal $f(t)$ from its wavelet representation, a condition must be satisfied by the wavelet $y(t)$, that is, if the wavelet $y(t)$ satisfies the *admissibility condition:*

$$C_\psi = \int_{-\infty}^{\infty} \frac{|\Psi(\omega)|^2}{|\omega|} d\omega < \infty,$$

with $\Psi(w)$ being the Fourier transform of $y(t)$, then the function $f(t)$ is recovered with the inverse continuous wavelet transform (ICWT) given by:

$$f(t) = \frac{1}{C_\psi} \int_{-\infty}^{\infty} \int_{-\infty}^{\infty} CWT_f(a,\tau) \cdot \psi_{a,\tau}(t) \frac{da\,d\tau}{a^2}$$

A straightforward interpretation of this expression is that any $f(t)$ can be written as a superposition of shifted and dilated wavelets.

Properties of the Continuous Wavelet Transform

Some basic properties of the continuous wavelet transform, which can be easily verified from the definition of this transform, are given in the following.

1.Linearity - follows from the linearity of the inner product.

2. Shift Property

If $g(t) = f(t-\tau') \Rightarrow CWT_g(a,\tau) = CWT_f(a,\tau-\tau')$.

3. Scaling Property

If $g(t) = \frac{1}{\sqrt{s}} f\left(\frac{t}{s}\right) \Rightarrow CWT_g(a,\tau) = CWT_f\left(\frac{a}{s}, \frac{\tau}{s}\right)$

4. Time Localization

The CWT of a Dirac pulse at time t_0 is: $CWT_d(a,t) = \frac{1}{\sqrt{a}} y^*\left(\frac{t_0 - t}{a}\right)$. Therefore the wavelet transform is equal to the scaled wavelet reversed in time and centered at the location of the Dirac.

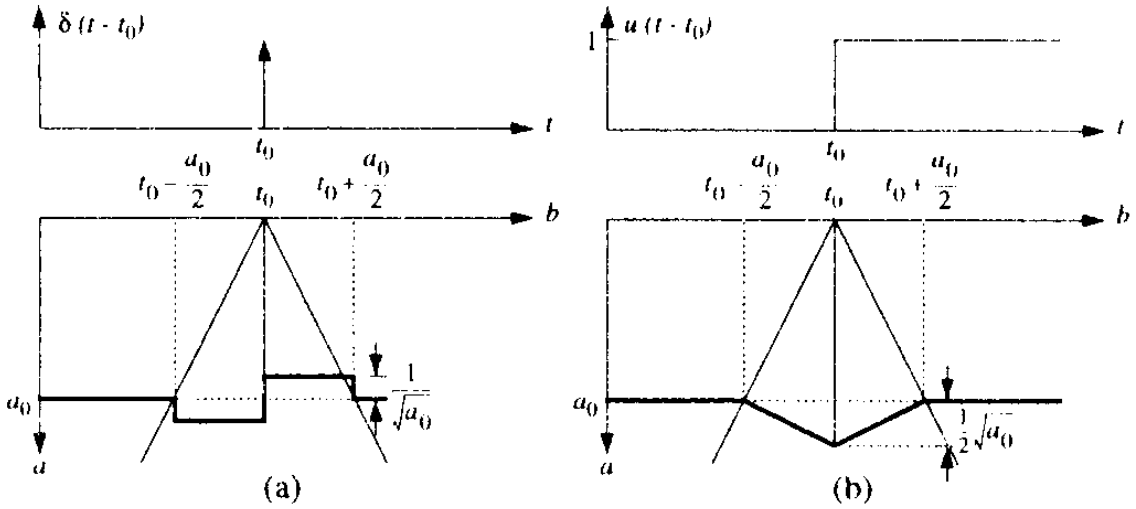

Figure 4.2.1. Time localization property, shown for the case of a zero-phase Haar wavelet. (a) Behavior of $f(t)=d(t-t_0)$. *The cone of influence has a width of* $a/2$ *on each side of* t_0 *and the height is* $a^{-1/2}$. *Behavior for* $f(t)=u(t-t_0)$, *that is, the unit-step function. The cone of influence is as in part (a), but the height is* $-1/2\,a_0^{1/2}$.

It is clear from the figure that the transform "zooms-in" to the Dirac with a very good localization for very small scales *a*.

5. Frequency Localization

Consider the sinc wavelet, a perfect bandpass filter with the magnitude 1 for $|w|\in[p,2p]$, and a complex sinusoide of unit magnitude at frequency w_0. From figure 4.2.2, we note that the highest frequency wavelet and the lowest frequency wavelet that can analyze the signal have a scale factor $a_{\min}=p/w_0$, respectively $a_{\max}=2p/w_0$.

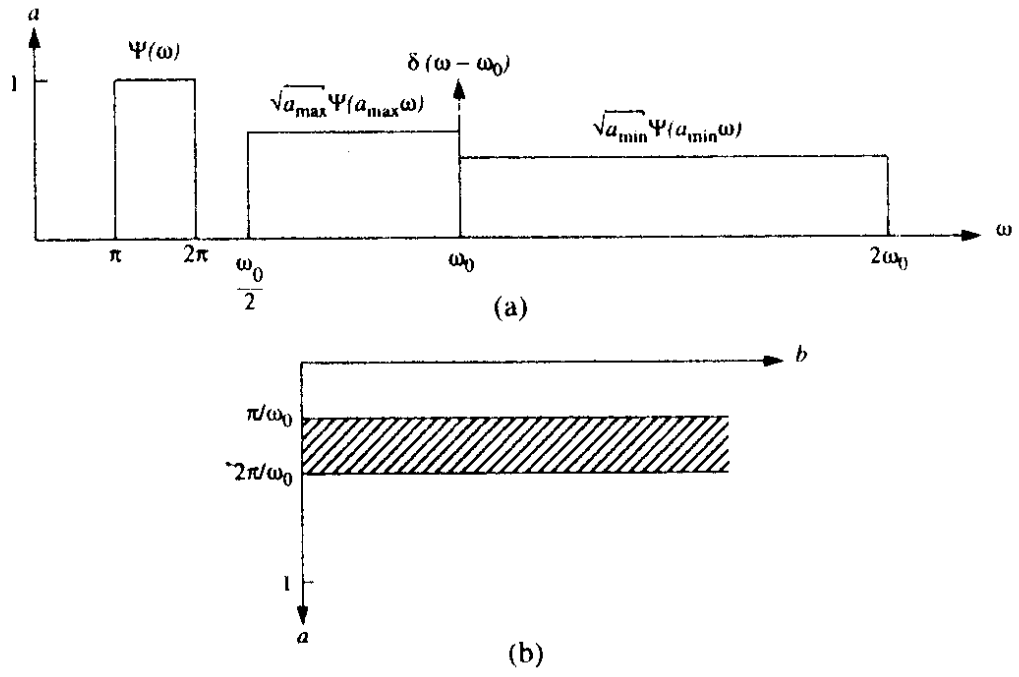

Figure 4.2.2. Frequency localization of the continuous wavelet transform using a sinc wavelet (a) Magnitude spectrum of the wavelet and its scaled versions involved in the resolution of a complex sinusoid at w_0. *(b) Nonzero magnitude of the continuous wavelet transform*

4.3. Frames of WT and STFT

The continuous short-time Fourier transform of a signal $f(t)$ is given by:

$$STFT_f(t,w) = \int_{-\infty}^{\infty} f(t)\cdot w^*(t-t)\cdot e^{-jwt}dt$$

As previously shown, this is equivalent with the inner product between the signal and the "shifts and modulates of the elementary window":

$STFT_f(\tau,\omega) = \langle f(t), g_{\omega,\tau}(t)\rangle$, where $g_{\omega,\tau}(t) = w(t-\tau)e^{j\omega t}$

The continuous wavelet transform of the signal $f(t)$ is given by:

$$CWT_f(a,t) = \frac{1}{\sqrt{a}}\int_{-\infty}^{\infty} f(t)\cdot y^*\left(\frac{t-t}{a}\right)dt$$

Similarly, if we write $y_{a,t}(t) = \frac{1}{\sqrt{a}}\cdot y\left(\frac{t-t}{a}\right)$, it is shown that the continuous wavelet transform measures actually the similarity between the signal and the scaled and shifted version of the elementary basis function $y(t)$:

$$CWT_f(a,t) = \langle f(t), y_{a,t}(t)\rangle$$

We notice from the expressions above that the signal as well as these two transforms are continuous in time. Since in practice we deal mostly with discrete signals (digital images), our interest is two derive the discrete versions of the transforms above. However, this problem is not as easy as it might appear, since to discretize these two transforms cannot simply be reduced to a discretization of a,t and w. To tackle this problem the approach followed by most of the authors in the literature was a classical one, similar to the one used in the Fourier case. Step 1: let us consider the signal *f* still continuous in time, discretize the transforms, represent the signal via a set of transform coefficients and reconstruct the signal in a stable way. Step 2: given the discrete versions of the two transforms, discretize the signal and derive the discrete-time series expansions for both short-time Fourier transform and wavelet transform.

The focus in this section is step 1, the problem to be solved being summarized as follows.

$$g_{w,t} \xrightarrow{\text{discretize } w,t} g_{m,n}, \quad \textit{such that} \quad f = \sum_m\sum_n \langle g_{m,n}, f\rangle \tilde{g}_{m,n}$$

$$y_{a,t} \xrightarrow{\text{discretize } a,t} y_{m,n}, \quad \textit{such that} \quad f = \sum_m\sum_n \langle y_{m,n}, f\rangle \tilde{y}_{m,n}$$

Discretizing the transforms leads to overcomplete continuous-time signal expansions called *frames*. They are sets of non-independent vectors that are able to represent every vector in a given space and are obtained by discretizing the continuous-time transforms (both wavelet and short-time Fourier transforms). We will see that a frame condition is necessary if we want a numerically stable reconstruction of a function *f* from a sequence of its transform coefficients (that is, $(\langle y_{m,n}, f\rangle)_{m,n\in Z}$ in the wavelet transform case, and $(\langle g_{m,n}, f\rangle)_{m,n\in Z}$ in the short-time Fourier transform case). The continuous-time wavelet and short-time Fourier transforms are extremely redundant, and sampling these transforms will lead to a smaller degree of redundancy. However, there will be a trade-off between oversampling and freedom in choosing our basis functions. In the most extreme case, for the short-time Fourier transform, the Balian-Low theorem tells us that when critical (Nyquist) sampling is used, it

will not be possible to obtain frames with good time and frequency resolutions. As a consequence, orthonormal short-time Fourier transform bases will not be achievable with basis functions being well localized in time and in frequency. On the other hand, wavelet frames are less restricted and this is one of the reasons behind the excitement that wavelets have generated over the past years.

4.3.1. Discretization of CWT

The set of basis functions for the continuous-time wavelet transform is:

$y_{a,b}(t) = \frac{1}{\sqrt{a}} y\left(\frac{t-b}{a}\right)$, where $a \in R^+, a \neq 0$ and $b \in R$.

The following discretization of the scaling parameter *a*, is chosen:

$a = a_0^{\,m}, m \in Z, a_0 \neq 1.$

As for the time shift *b*, consider the following: for $m = 0,$ discretize b by taking integer multiples ($b = nb_0$) of a fixed $b_0, b_0 > 0$. The step b_0 should be chosen in such a way that $y_{1,b} = y(t - nb_0)$ "covers" the whole time axis. Moreover, the step size *b* at scale *m* cannot be chosen independently of *m*, since the basis functions are rescaled. Therefore, for any scale *m*, we should choose b_0 such that $y_{a_0^{\,m},b}(t)$ covers the whole time axis. If we define the "width" $\Delta_t(f)$ of the function *f*, due to rescaling one can write: $\Delta_t\left(y_{a_0^{\,m},0}(t)\right) = a_0^{\,m}\Delta_t\left(y_{1,0}(t)\right)$. Then, it is obvious that for $y_{a,b}(t)$ to "cover" the whole time axis at a scale $a = a_0^{\,m}$, the shift has to be $b = nb_0 \cdot a_0^{\,m}$. In summary, the following discretization is chosen:

$a = a_0^{\,m}$ *and* $b = nb_0 a_0^{\,m}, \quad m, n \in Z, \quad a_0 > 1, b_0 > 0$

The discretized family of wavelets is now: $y_{m,n}(t) = a_0^{\,-m/2} y\left(a_0^{\,-m} t - nb_0\right)$

As illustrated in figure 4.3.1.1, to different values of *m* correspond wavelets of different widths. Narrow, high-frequency wavelets are translated by smaller steps in order to "cover" the whole time axis, while wider, low-frequency wavelets are translated by larger steps.

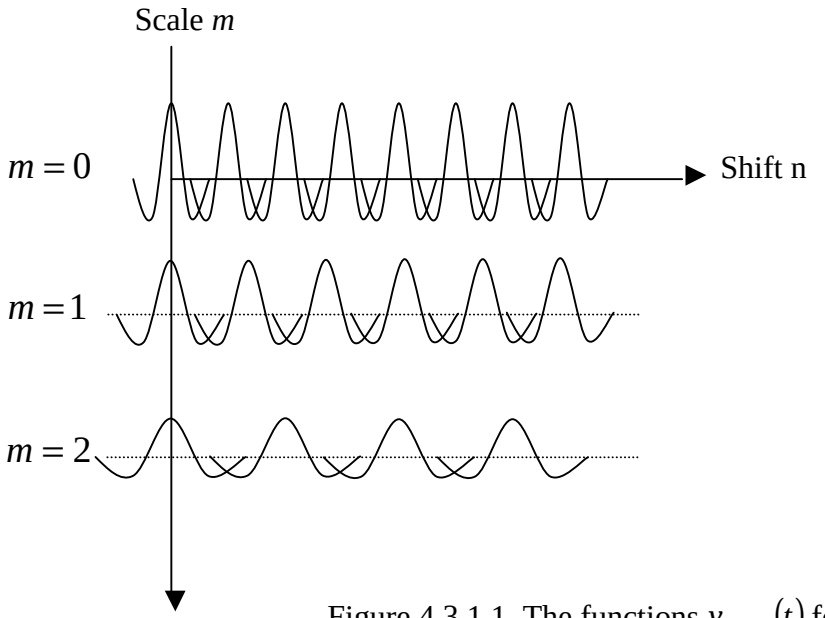

Figure 4.3.1.1. The functions $y_{m,n}(t)$ for $a_0 = 2^{-1/2}$ and $b_0 = 1$

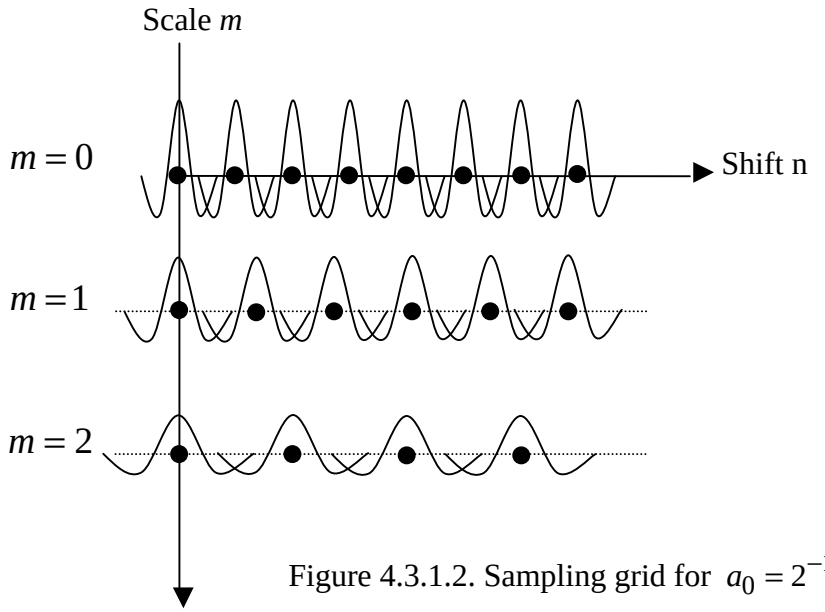

Figure 4.3.1.2. Sampling grid for $a_0 = 2^{-1/2}$ and $b_0 = 1$

By discretizing the values of the scaling and shift parameters $a = a_0^{\,m}$ *and* $b = nb_0a_0^{\,m}$, one obtains the sampling grid shown in figure 4.3.1.2 (black dots indicate the sampling grid).
We would like to answer the following question: given the sequence of transform coefficients $\langle y_{m,n}, f \rangle$ is it possible to reconstruct *f* in a numerically stable way? In section 4.3.3 it will be shown that when the parameters are discretized, the reconstruction is possible provided that $(y_{m,n})_{m,n\in Z}$ constitute a frame. Then, for certain y and appropriate a_0, b_0, there exist $\tilde{y}_{m,n}$ such that the function *f* can be reconstructed as follows:

$$f = \sum_m \sum_n \langle y_{m,n}, f \rangle \tilde{y}_{m,n}$$

4.3.2. Discretization of STFT

The set of basis functions for the short-time Fourier transform is:

$g_{w,t}(t) = e^{jwt} w(t - t)$.

In the same manner as for the wavelet transform, it is possible to discretize the short-time Fourier transform as follows:

- Discretization of the frequency parameter

$w = mw_0,\ w_0 > 0,\ m \in Z, w_0$ *fixed*

- Discretization of the time shift

$t = nt_0,\ t_0 > 0,\ n \in Z, t_0$ *fixed*

The resulting set of discrete basis functions is given by:

$$g_{w,t}(t) \to g_{m,n}(t) = e^{jmw_0 t} w(t - nt_0)$$

Note that for any *m*, the time-frequency resolution of each basis function is constant, that is:
$\Delta_t(g_{m,0}(t)) = \Delta_t(g_{1,0}(t))$ and $\Delta_w(g_{m,0}(t)) = \Delta_w(g_{1,0}(t))$.
By discretizing the frequency and shift parameters one obtains the sampling grid shown in figure 4.3.2.1 (black dots indicate the sampling grid). Note that due to the constant time-frequency resolution of the discrete basis functions, the STFT sampling grid is different than the sampling grid obtained from the discretization of the continuous-time wavelet transform (see figure 4.3.1.2).

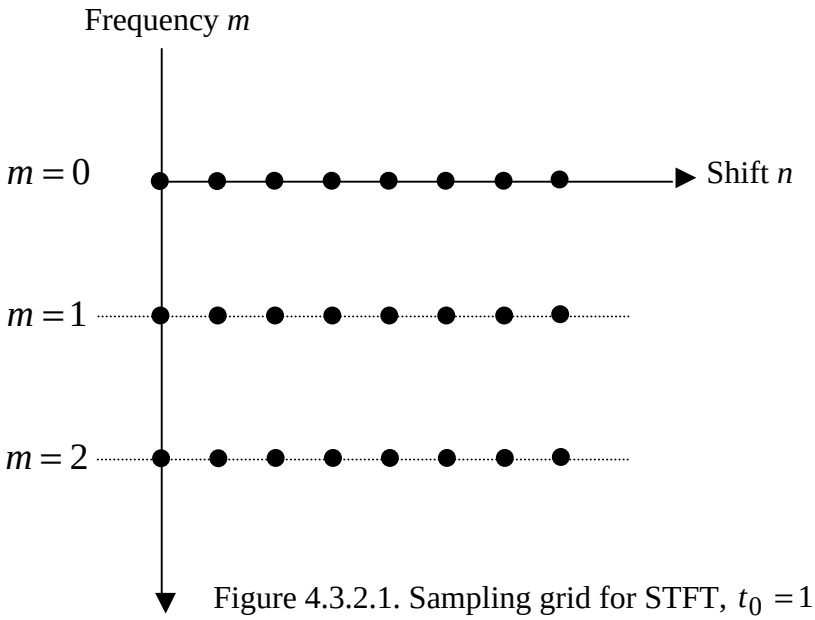

Figure 4.3.2.1. Sampling grid for STFT, $t_0 = 1$

Again, we would like to know in which conditions it is possible to reconstruct a given function f from its transform coefficients $\left(\langle g_{m,n}, f \rangle\right)_{m,n}$ in a numerically stable way, and again, the answer is positive provided that $\left(g_{m,n}\right)_{m,n \in Z}$ constitute a frame (this will be shown in the next section). Then, for certain g and appropriate w_0, t_0, there exist $\tilde{g}_{m,n}$ (called the *dual frame*) such that:

$$\sum_m \sum_n \langle g_{m,n}, f \rangle \, \tilde{g}_{m,n} = f = \sum_m \sum_n \langle \tilde{g}_{m,n}, f \rangle \, g_{m,n}$$

4.3.3. Reconstruction in Frames

Let us now see what is necessary in order to have a numerically stable reconstruction in the case of the discretized CWT; following a similar reasoning, the necessary conditions are derived for the discretized STFT.

Intuitively, the operator that maps a function $f(t)$ into a set of coefficients $\left(\langle y_{m,n}, f \rangle\right)_{m,n}$ has to be bounded. That is, if $f(t) \in L^2(R)$, then $\sum_{m,n} \left|\langle y_{m,n}, f \rangle\right|^2$ has to be finite. Also, no $f(t)$ with $\|f\| > 0$ should be mapped to 0. These two conditions lead to the *frame bounds*, which guarantee a stable reconstruction.

1. Consider the first condition. For any wavelet with some decay in time and frequency, having zero mean, and any choice of $a_0 > 1, b_0 > 0$, it can be shown that it exists a constant B, such that:

   $\sum_{m,n} \left|\langle y_{m,n}, f \rangle\right|^2 \le B \|f\|^2$.

   This condition just states that the sequence $\left(\langle y_{m,n}, f \rangle\right)_{m,n}$ is in $l^2\left(Z^2\right)$, that is the sequence is square-summable.

2. On the other hand, the requirement for stable reconstruction means that if $\|f\|^2$ is small, $\sum_{m,n}\left|\langle y_{m,n}, f\rangle\right|^2$ should be small as well (that is, $\sum_{m,n}\left|\langle y_{m,n}, f\rangle\right|^2$ should be "close" to $\|f\|^2$). This further means that if $\sum_{m,n}\left|\langle y_{m,n}, f\rangle\right|^2 < 1$, there should exist $a < \infty$ such that $\|f\|^2 < a$. Define $\tilde{f} = \frac{f}{\sqrt{\sum_{m,n}\left|\langle y_{m,n}, f\rangle\right|^2}}$. If the reconstruction is stable for f, then it is stable also for $\tilde{f}$. That is, $\sum_{m,n}\left|\langle y_{m,n}, \tilde{f}\rangle\right|^2 \le 1 \Rightarrow \exists a'$, such that $\|\tilde{f}\|^2 \le a' \Leftrightarrow \frac{1}{a'}\|f\|^2 \le \sum_{m,n}\left|\langle y_{m,n}, f\rangle\right|^2$, and making the notation $A = \frac{1}{a'}$, this leads to $A\cdot\|f\|^2 \le \sum_{m,n}\left|\langle y_{m,n}, f\rangle\right|^2$.

Putting the two conditions together tells us that a numerically stable reconstruction of *f* from its transform (wavelet) coefficients is possible if and only if:

$$\exists A, B,\ 0 < A \le B < \infty, \quad A\cdot\|f\|^2 \le \sum_{m,n}\left|\langle y_{m,n}, f\rangle\right|^2 \le B\cdot\|f\|^2$$

If this condition is satisfied, then the family $(y_{m,n})_{m,n\in Z}$ *constitutes a frame.*

- Note: take $f = f_1 - f_2$. First inequality means that the distance $\|f_1 - f_2\|$ cannot be arbitrarily large if $\sum_{m,n}\left|\langle y_{m,n}, f_1\rangle - \langle y_{m,n}, f_2\rangle\right|^2$ is small; this is the *stability* requirement.
- Note: when $A = B$, the frame is *tight*; *A* and *B* are called *frame bounds*.

Proposition.

- If $A = B = 1$ and $\forall m, n \in Z$, $\|y_{m,n}\| = 1$, then the family $(y_{m,n})_{m,n\in Z}$ forms an *orthonormal basis*.
  - *A* = *B* gives the "redundancy ratio", or the oversampling ratio.
  - If *A* = *B* = 1 we obtain the "critical" (Nyquist) sampling case, or an orthonormal basis. The converse is just the Parseval formula, that is, an orthonormal basis is also a tight frame with frame bounds equal to 1.

A. **Reconstruction in tight frames**

As we have just seen, for numerically stable reconstruction, the vectors used for the expansion have to constitute a frame. In the following we will briefly discuss the frames, and we will focus on the algorithm needed to reconstruct *f* from its transform coefficients. For a more detailed and rigorous account of frames, the reader should consult [3], [4].

For tight frames *A* = *B*, therefore:

$$\sum_{m,n}\left|\langle y_{m,n}, f\rangle\right|^2 = A\|f\|^2 \Leftrightarrow \sum_{m,n}\langle f, y_{m,n}\rangle\cdot\langle y_{m,n}, f\rangle = A\langle f, f\rangle$$

$$\sum_{m,n}\langle f, y_{m,n}\rangle\cdot\langle y_{m,n}, f\rangle = \sum_{m,n}\langle f, y_{m,n}\rangle\cdot\int y_{m,n}^{*}(t) f(t) dt =$$

$$= \int\left(\sum_{m,n}\langle f, y_{m,n}\rangle\cdot y_{m,n}(t)\right)^{*}\cdot f(t)dt = \left\langle\sum_{m,n}\langle f, y_{m,n}\rangle^{*}\cdot y_{m,n}, f\right\rangle = A\langle f, f\rangle \Rightarrow$$

$$f = \frac{1}{A}\sum_{m,n}\left\langle f, y_{m,n}\right\rangle^{*} \cdot y_{m,n} = \frac{1}{A}\sum_{m,n}\left\langle y_{m,n}, f\right\rangle \cdot y_{m,n}\,.$$

This gives us an easy way to recover *f* from its transform coefficients $\left(\left\langle y_{m,n}, f\right\rangle\right)_{m,n}$ if the frame is tight. Note that the formula above with $A = 1$ gives the usual reconstruction formula for an orthonormal basis.

It is important to note that *a frame, however, even a tight frame is not an orthonormal basis*; it is a *set of non-independent vectors,* as it is shown in the following example.

Example. Consider R^2 and a redundant set of vectors:

$$j_0 = [1,0]^T,\ j_1 = \left[-1/2, \sqrt{3}/2\right]^T,\ j_2 = \left[-1/2, -\sqrt{3}/2\right]^T$$

$$\forall x \in R^2,$$

Create a matrix $M = [j_0, j_1, j_2]$. It is easy to verify that $MM^T = \frac{3}{2}I$, therefore any vector $x \in R^2$ can be written as a linear combination of the vectors j_i, $i = 0,1,2$:

$$x = \frac{2}{3}\sum_{i=0}^{2}\langle j_i, x\rangle j_i = \frac{1}{3/2}\sum_{i=0}^{2}\langle j_i, x\rangle j_i\,.$$

Note from this formula that the vectors of the dual frame are $\tilde{j}_i = j_i$, $i = 0,1,2$. Note also that $\|j_i\|_{i=0,1,2} = 1$ and that $A = 3/2$ is the redundancy ratio (see the reconstruction formula above).

However, the vectors j_i are linearly dependent, since $\exists\, a, b$ such that (for example) $j_0 = a \cdot j_1 + b \cdot j_2$; it is easy to find in this case that $a = b = -1$. Since the vectors j_i are linearly dependent, the set j_i used to transform *x* (or in equivalent terms, to perform the "analysis") is not unique. Also, the set $\tilde{j}_i$ used to reconstruct *x* (or in equivalent terms, to perform the "synthesis") is not unique either. As an example, one can choose:

$$\tilde{j}_i = j_i + \begin{bmatrix} a \\ b \end{bmatrix},$$

and still obtain $x = \frac{2}{3}\sum_{i=0}^{2}\langle j_i, x\rangle \tilde{j}_i = \frac{1}{3/2}\sum_{i=0}^{2}\langle j_i, x\rangle \tilde{j}_i$. The proof is immediate:

$$\frac{2}{3}\sum_{i=0}^{2}\langle j_i, x\rangle \tilde{j}_i = \frac{2}{3}\sum_{i=0}^{2}\langle j_i, x\rangle j_i + \frac{2}{3}\sum_{i=0}^{2}\langle j_i, x\rangle \begin{bmatrix} a \\ b \end{bmatrix} = x + \frac{2}{3}\sum_{i=0}^{2}\langle j_i, x\rangle \begin{bmatrix} a \\ b \end{bmatrix} =$$

$$= \begin{bmatrix} x_1 \\ x_2 \end{bmatrix} + \frac{2}{3}\left(x_1 + \frac{-x_1 + \sqrt{3}x_2}{2} + \frac{-x_1 - \sqrt{3}x_2}{2} \right)\begin{bmatrix} a \\ b \end{bmatrix} = x$$

The particular choice of $a = b = 0$ leads to $\tilde{j}_i = j_i$, $i = 0,1,2$ as above.

Once again, this example illustrates that a tight frame is a set of non-independent vectors (even with unity norm), and not necessarily an orthonormal set of vectors. A tight frame is an orthonormal basis if the vectors in the basis have a unity norm and if the redundancy ratio is 1.

B. **Reconstruction in frames that are not tight**

Proposition. Given a family of functions $\left(g_j\right)_{j \in J}$ that constitutes a *non-tight frame* in a Hilbert space *H*, satisfying:

$$A\|f\|^2 \le \sum_{j\in J} \left|\langle g_j, f\rangle\right|^2 \le B\|f\|^2,$$

then it can be proven that it exists a family of functions $(\tilde{g}_j)_{j\in J}$ called a *dual frame*, satisfying:

$$B^{-1}\|f\|^2 \le \sum_{j\in J} \left|\langle \tilde{g}_j, f\rangle\right|^2 \le A^{-1}\|f\|^2, \text{ and } f = \sum_{j\in J} \langle g_j, f\rangle \tilde{g}_j = \sum_{j\in J} \langle \tilde{g}_j, f\rangle g_j .$$

The first condition shows that the frame bounds for $(\tilde{g}_j)_{j\in J}$ are $1/B$ and $1/A$ respectively, and the second condition is the reconstruction formula for frames that are not tight. For a proof of this theorem and related issues the reader is referred to [5].

4.3.4. Frames of the CWT

This section discusses some particularities of frames of the wavelet transform, the main point being the fact that for wavelet frames there are no really strong constraints on $y(t), a_0, b_0$.

A family of wavelets being a frame imposes the admissibility condition for the "mother" wavelet. The result is given without a proof in the following proposition (for a proof, refer to [4]).

Proposition. If $y_{m,n}(t) = a_0^{-m/2} y\left(a_0^{-m} t - n b_0\right), m, n \in Z$ constitute a frame in $L^2(R)$ with frame bounds *A*, *B*, then:

$$\frac{b_0 \ln a_0}{2p} A \le \int_0^\infty \frac{|\Psi(w)|^2}{w} dw \le \frac{b_0 \ln a_0}{2p} B \quad \text{and} \quad \frac{b_0 \ln a_0}{2p} A \le \int_{-\infty}^0 \frac{|\Psi(w)|^2}{|w|} dw \le \frac{b_0 \ln a_0}{2p} B$$

Compare these two inequalities with the admissibility condition:

$$C_y = \int_{-\infty}^{\infty} \frac{|\Psi(w)|^2}{|w|} dw < \infty$$

It is obvious that the fact that the wavelets form a frame automatically imposes the admissibility condition on the mother wavelet. This proposition helps us to find the frame bounds for a tight frame:

$$A = B = \frac{2p}{b_0 \ln a_0} \int_0^\infty \frac{|\Psi(w)|^2}{w} dw = \frac{2p}{b_0 \ln a_0} \int_{-\infty}^0 \frac{|\Psi(w)|^2}{|w|} dw$$

Moreover, for orthonormal bases and taking the dyadic case ($b_0 = 1, a_0 = 2$) as example, the wavelet should satisfy:

$$A = B = 1 \Rightarrow \quad \int_0^\infty \frac{|\Psi(w)|^2}{w} dw = \int_{-\infty}^0 \frac{|\Psi(w)|^2}{|w|} dw = \frac{\ln 2}{2p}$$

We mentioned previously that in order to have wavelet frames, we do not need to impose strong conditions on the wavelet, and the scaling and shift factors. In other words, if $y(t)$ is at all a "reasonable" function (with some decay in time and in frequency, and $\int y(t) dt = 0$), then there exists a whole arsenal of a_0, b_0 such that $\{y_{m,n}\}$ constitute a frame. This can be formalized and we refer to [4] in which explicit estimates for the frame bounds *A*,*B*, as well as possible choices for $y(t), a_0, b_0$ are given.

As an example to the previous discussion, consider the so-called Mexican-hat function:

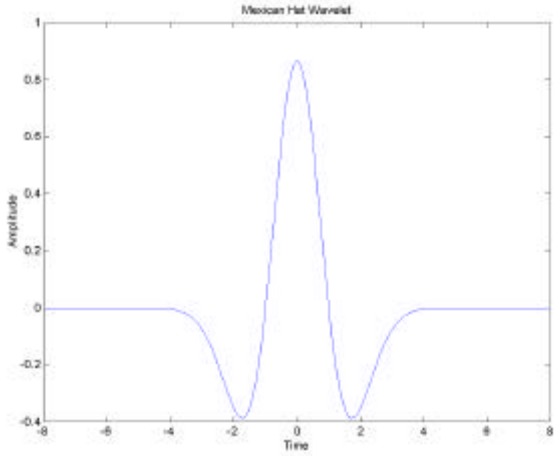

Figure 4.3.4.1. The Mexican-hat function $y(t)$. The rotated $y(t)$ gives rise to a mexican hat, thus the name for the function.

b_0	A	B	B/A
0.25	13.091	14.183	1.083
0.50	6.546	7.092	1.083
0.75	4.364	4.728	1.083
1.00	3.223	3.596	1.116
1.25	2.001	3.454	1.726
1.50	0.325	4.221	12.986

Table 4.3.4.1. Frame bounds for Mexican-hat wavelet frames for $a_0 = 2$ and different values of b_0 (from [4]).

$y(t) = \frac{2}{\sqrt{3}} p^{-1/4}\left(1-t^2\right)e^{-t^2/2}$, given in figure 4.3.4.1.

Table 4.3.4.1 gives a few values for the frame bounds *A* and *B* for Mexican-hat wavelet frames considering $a_0 = 2$ and different choices of b_0. Note for example that for some values of b_0 the frame is almost tight. When the frame is almost tight, the frame bounds are inversely proportional to b_0; when b_0 is halved (twice as many points on the grid), the frame bounds should double - redundancy increases by two since we have twice as many functions. Note also how for $b_0 = 1.50$, the ratio B/A increases suddenly. Actually, for larger values of b_0 the set $\{y_{m,n}\}$ is not even a frame anymore, since *A* is not strictly positive anymore.

Finally, let us say a few words on time-frequency localization properties of wavelet frames. Recall that one of the reasons we opted for the wavelet-type signal expansion is because they allegedly provide good localization in both time and frequency. Let us here assume that $|y|$ and $|\Psi|$ are symmetric and centered about t = 0 and $\omega = \omega_0$. This implies that $y_{m,n}$ is centered around $t = a_0^{\,m} n b_0$ in time and around $w = \pm a_0^{\,-m} w_0$ in frequency (see figures 4.3.4.2a-b).

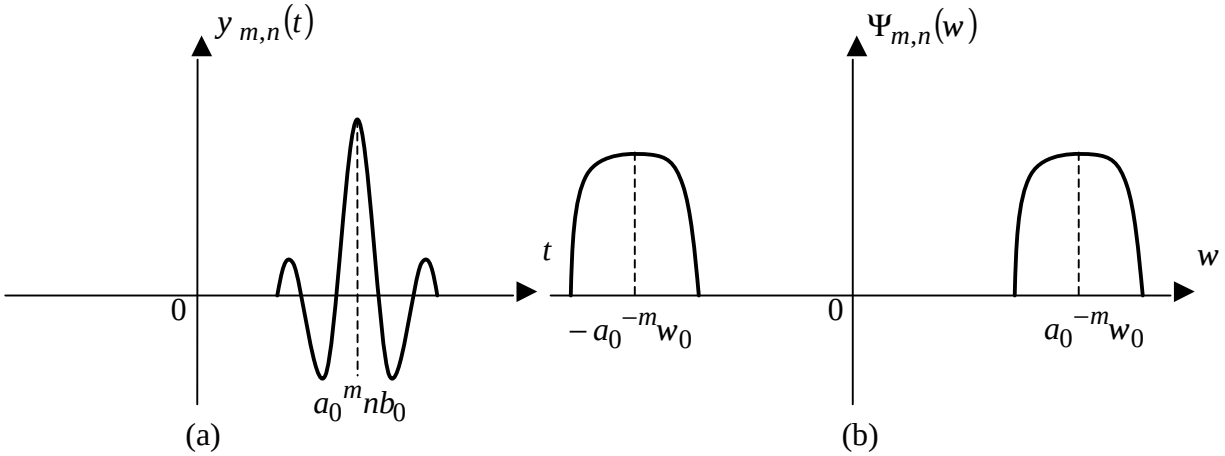

Figure 4.3.4.2. The wavelet $y_{m,n}$ is centered around (a) $t = a_0^{\,m} n b_0$ in time and around (b) $w = \pm a_0^{\,-m} w_0$ in frequency.

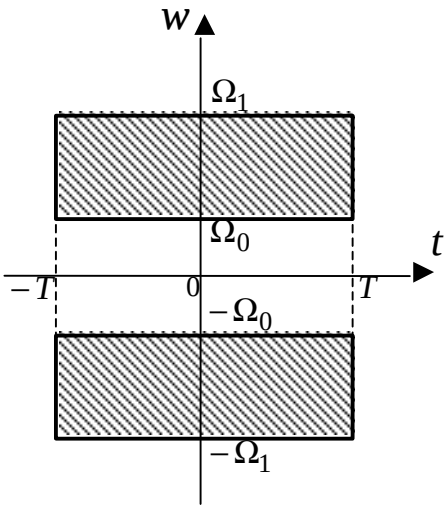

Figure 4.3.4.3. Time-frequency representation for the function f whose energy lies within $|t| \le T$ and $\Omega_0 \le |w| \le \Omega_1$ respectively.

This means that the inner product $\langle y_{m,n}, f \rangle$ represents the "information content" of f near $t = a_0^{\,m} n b_0$ and near $w = \pm a_0^{\,-m} w_0$.

Assume that the function f is localized both in time and in frequency, that is, most of its energy lies within $|t| \le T$ and $\Omega_0 \le |w| \le \Omega_1$, as depicted in figure 4.3.4.3. Then only the coefficients $\langle y_{m,n}, f \rangle$ for which $(t,w) = \left(a_0^{\,m} n b_0, a_0^{\,-m} w_0\right)$ lies within (or very close) to $[-T,T] \times ([-\Omega_1,-\Omega_0] \cup [\Omega_0,\Omega_1])$ are needed for f to be reconstructed up to a very good approximation. For details concerning this approximation property, the reader is referred to [4].

4.3.5. Frames of the STFT

Let us turn our attention to the short-time Fourier transform frames. In contrast to the wavelet transform, the situation is more complicated for the short-time Fourier transform and having good frames will be possible only for certain choices of w_0 and t_0. Moreover, if we want to avoid redundancy and critically sample the STFT, we will have to give up either good time or good frequency resolution. This is the content of the Balian-Low theorem, given in this section.

In a similar way as for the wavelet transform, the following proposition can be formulated (see [4] for proof).

Proposition. If $g_{m,n}(t)$ constitute a frame for $L^2(R)$ with frame bounds A and B, then:

$$A \le \frac{2p}{w_0 t_0} \|g\|^2 \le B .$$

Note from this expression that in contrast with the wavelet frames, g does not appear, except $\|g\|$ which can always be normalized to 1. The direct result is that there is no admissibility condition for STFT frames as it exists for the wavelet frames. Note also how in this case any tight frame will have a frame bound $A = B = 2p/(w_0 t_0)$ (for $\|g\| = 1$). In particular an orthonormal basis will require the following to be true:

$w_0 t_0 = 2p$

Beware, however, that $w_0 t_0 = 2p$ will not imply an orthonormal basis, this condition simply states that we have "critically" sampled our short-time Fourier transform. Moreover, we see

that w_0 and t_0 cannot be arbitrarily chosen (see figure 4.3.5.1). In fact there are no short-time Fourier transform frames for $w_0 t_0 > 2p$. Moreover, in order to have good time-frequency localization, we require that $w_0 t_0 < 2p$. The last remaining case, that of critical sampling, $w_0 t_0 = 2p$, is very interesting. Unlike for the wavelet frames, it turns out that no critically sampled short-time Fourier transform frames are possible with good time and frequency localization. The following theorem states just that.

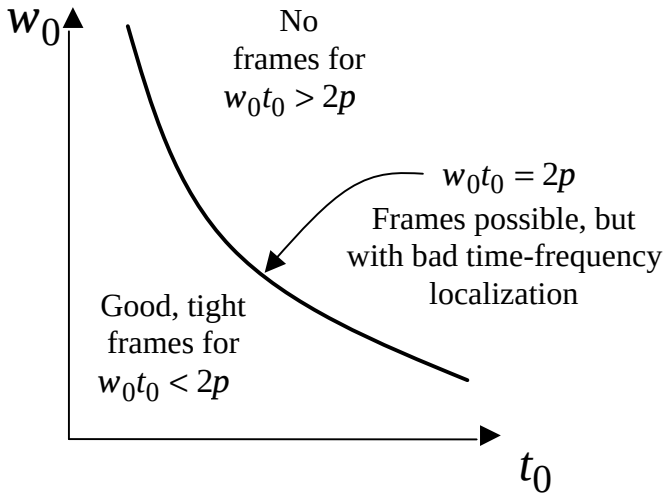

Figure 4.3.5.1. STFT case: no frames are possible for $w_0 t_0 > 2p$; there exists frames with bad time-frequency localization for $w_0 t_0 = 2p$; frames (even tight frames) with excellent localization properties are possible for $w_0 t_0 < 2p$ (after [4]).

Theorem (Balian-Low). If the $g_{m,n}(t) = e^{j2pmt} w(t-n), m, n \in Z$ constitute a frame for $L^2(R)$ with frame bounds *A* and *B*, then either $\int t^2 |w(t)|^2 dt = \infty$ either $\int w^2 |W(w)|^2 dw = \infty$; for a proof see [4].

Note that the settings in the statement of the theorem are $w_0 = 2p$ and $t_0 = 1 \Rightarrow w_0 t_0 = 2p$. The result of this theorem shows that in the case $w_0 t_0 = 2p$ (critical sampling) we will necessarily have bad localization either in time or in frequency (or possibly both). This theorem has profound consequences, since it also implies that no good short-time Fourier transform orthonormal bases (good meaning with good time and frequency localization) are achievable: orthonomal bases are necessarily critically sampled, and this requirement settles us on the curve in figure 4.3.5.1.

To conclude this section, we will consider an example from [4] considering the Gaussian window, where it can be shown how the dual frame needed for reconstruction starts to "misbehave" as oversampling approaches critical sampling.

Example.

Consider a Gaussian window: $w(t) = p^{-1/4} e^{-t^2/2}$ and the family of functions $g_{m,n}(t) = e^{jmw_0 t} w(t - nt_0)$, constituting a frame. Consider the choice when $w_0 = t_0 = (2p\,l)^{1/2}$, or $w_0 t_0 = 2p\,l$. Note that this family of functions constitutes a frame for $w_0 t_0 < 2p$, which is equivalent to $l < 1$, and critical sampling is achieved for $l = 1$ ($w_0 t_0 = 2p$).

It can be shown (see [5] for a proof) that the dual frame is of the form:

$\tilde{g}_{m,n}(t) = e^{jmw_0 t} \tilde{w}(t - nt_0)$.

The window $\tilde{w}(t)$ is calculated in [5] using an iterative procedure. The interesting part of this example which constitutes itself as a good ilustration of the Balian-Low theorem comes from the plots of $\tilde{w}(t)$ (obtained for different values of l) shown in figure 4.3.5.2.

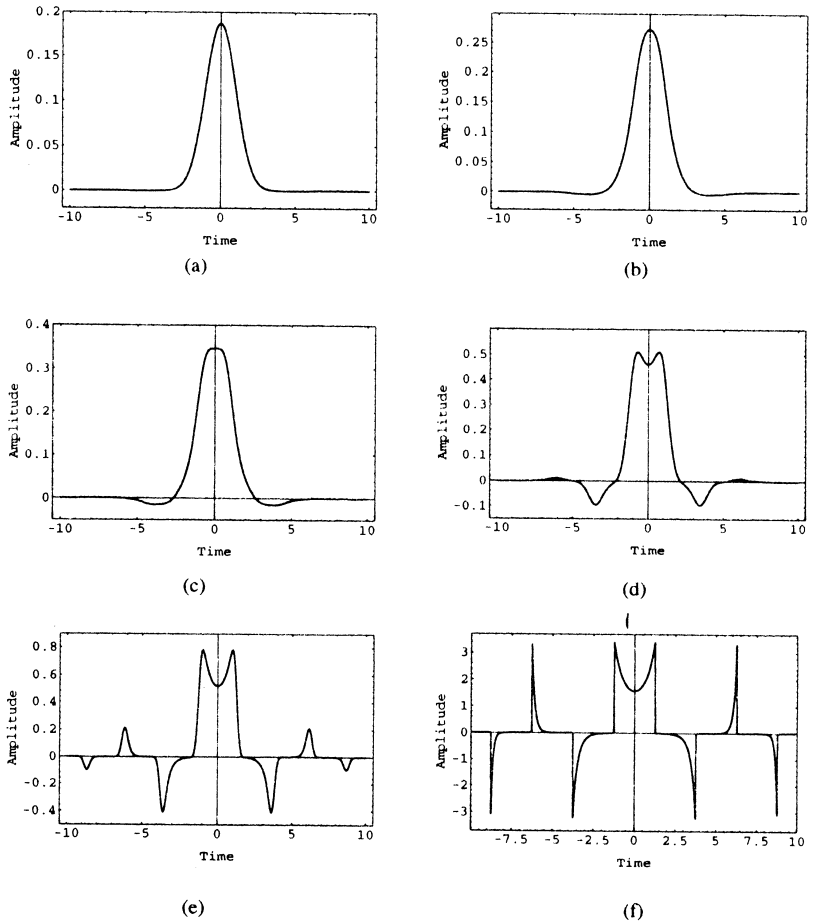

Figure 4.3.5.2. The dual frame functions $\tilde{w}$ for $w_0 = t_0 = \sqrt{2pl}$ and (a) λ = 0.25; (b) λ = 0.375; (c) λ = 0.5; (d) λ = 0.75; (e) λ = 0.95; (f) λ = 1.00 (after [4]).

As shown in this figure, for small values of l (e.g. λ = 0.25, which is equivalent to a degree of redundancy equal to $1/l = 4$), the windows $\tilde{w}(t)$ are smooth. However, as the value of l increases (oversampling decreases), the dual frame functions $\tilde{w}(t)$ are less and less smooth. Even so, for $l < 1$, these dual frame have good localization properties. However, for λ = 1.00 (equivalent to critical sampling), $\tilde{w}(t)$ is not even square-integrable anynmore.

We conclude from this example what the Balian-Low theorem stated before: it is not possible to obtain STFT frames with good time and frequency localization properties, and consequently orthonormal STFT bases are not be achievable with basis functions being well localized in time and in frequency. To avoid the drawbacks stated by the Balian-Low theorem, several authors have used modulation by cosines instead of modulation by complex exponentials in the short-time Fourier transform, this approach yielding good orthonormal bases called local cosine bases.

5. The Multiresolution Representation

5.1. Multiresolution Analysis – Multiresolution Approximation of $L^2(R)$

The basic idea of the multiresolution analysis is to represent any arbitrary function f$\in L^2(R)$ as a set of successive approximations of the original function.

Let A_j be the operator which approximates a signal at the resolution 2^j. We will consider $j<0$, since starting from an original signal at resolution 2^0 (i.e. $j=0$), we can only construct approximations at lower resolutions. In multiresolution analysis we only consider particular scale values, namely $a=2^{-j}$, corresponding to resolutions 2^j, $j<0$. Suppose that the original signal $f(x)$ is measurable and has finite energy: $f(x)\in L^2(R)$. We characterize in the following the operator $A_j f$ from the intuitive properties that one would expect from such an approximation operator.

1. A_j is a linear operator. If $A_j f(x)$ is the approximation of the function $f(x)$ at the resolution 2^j, then $A_j f(x)$ is not modified if we approximate it again at the resolution 2^j. This principle shows that $A_j \circ A_j = A_j$. Let $V_j \subset L^2(R)$ be the vector space of all possible approximations at the resolution 2^j of the functions in $L^2(\mathrm{R})$. Thus, the operator A_j is the projection operator on the vector space V_j.
2. Among all the approximated functions at the resolution 2^j, $A_j f(x)$ is the function which is the most similar to $f(x)$ in the least square sense:

$\forall g(x)\in L^2(R), \|g(x)-f(x)\| \geq \left\|A_j f(x)-f(x)\right\|$, where $\|\ \|$ is the norm in $L^2(\mathrm{R})$.

3. The approximation of $f(x)$ at the resolution 2^{j+1} contains all the necessary information to compute the same signal at smaller resolution 2^j. Since A_j is the projection operator in V_j this principle is equivalent to:
   $V_j \subset V_{j+1}, \forall j \in Z$. Remark that:
   $...V_{j-1} \subset V_j \subset V_{j+1} \subset ...$

Since the approximation operator A_j is the projection operator on the vector space V_j, we can characterize this operator by finding an orthonormal basis in V_j. The following theorem shows that we can define an orthonormal basis in V_j by scaling and translating a unique function $\phi(x)$.

Theorem 1. There exist a unique function $\phi(x)\in L^2(R)$, called a *scaling function,* such that if $\phi_j(x)=2^j\phi\left(2^j x\right)$ is the dilation at the scale 2^j then $\left(\sqrt{2^{-j}}\phi_j\left(x-2^{-j}n\right)\right)_{n\in Z}$ is an orthonormal basis of V_j.

An example of a scaling function is given in figure 5.1.1.

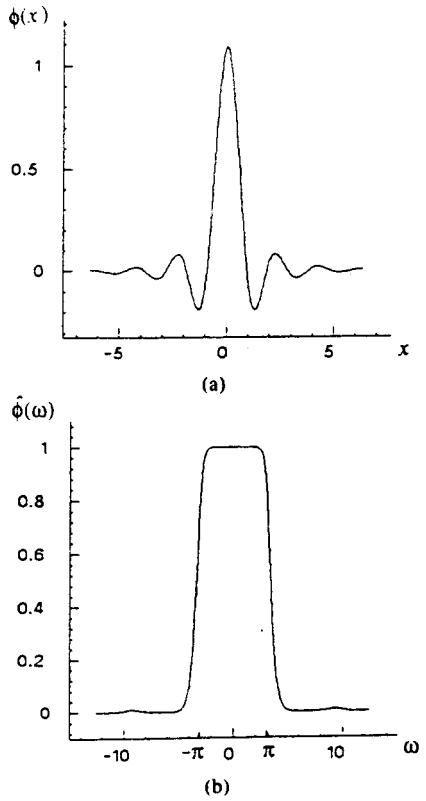

Figure 5.1.1. (a) Example of a scaling function $\phi(x)$. *(b) Modulus of the Fourier transform* $\Phi(\omega)$. *A scaling function is a low pass filter.*

Therefore, the orthogonal projection $A_j f(x)$ can be computed by decomposing the signal on the orthonormal basis given by theorem1:

$$\forall f(x) \in L^2(R),\ A_j f(x) = 2^{-j} \sum_{n=-\infty}^{\infty} \left\langle f(u),\ f_j\left(u - 2^{-j} n\right)\right\rangle f_j\left(x - 2^{-j} n\right).$$

The approximation of the function $f(x)$ at the resolution 2^j, $A_j f(x)$, is thus characterized by the set of inner products which we denote by:

$$A_j^d f(n) = \left(\left\langle f(u),\ f_j\left(u - 2^{-j} n\right)\right\rangle \right)_{n \in Z}.$$

$A_j^d f$ is called a *discrete approximation* of $f(x)$ at the resolution 2^j.

The continuous and the discrete approximations of a signal at several resolutions are given in figure 5.1.2.

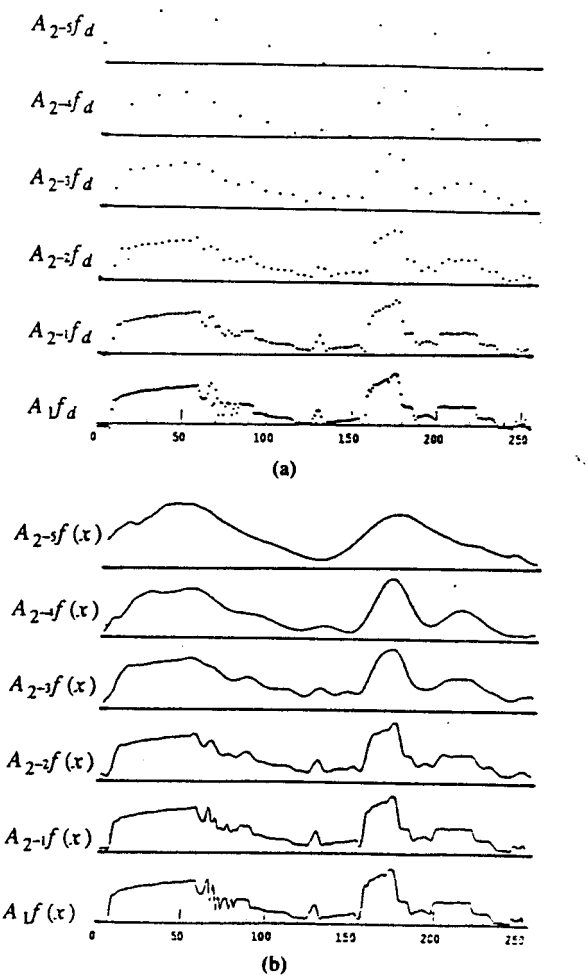

Figure 5.1.2. (a) Discrete approximations $A_j^d f$ *(or* $A_{2^j}^d f$ *in the figure) at the resolutions* $1, 1/2, 1/4, 1/8, 1/16$ *and* $1/32$*. (b) Continuous approximations* $A_j f$ *(or* $A_{2^j} f$ *in the figure) at the resolutions* $1, 1/2, 1/4, 1/8, 1/16$ *and* $1/32$*;* $A_0 f(x)$ *(or* $A_1 f(x)$ *in the figure) is the original signal.*

It is shown in the following that all these approximations can be computed using a pyramidal algorithm.
Define the discrete filter *H* whose impulse response is given by:

$$\forall n \in Z, \quad h(n) = \langle \phi_{-1}(u), \phi(u-n) \rangle,$$

and $\tilde{H}$ the mirror filter given by $\tilde{h}(n) = h(-n)$. The discrete approximation of $f(x)$ at the resolution 2^j, $A_j^d f$, can be computed by convolving $A_{j+1}^d f$ with $\tilde{H}$ and keeping every other sample of the output (downsampling by 2):

$$A_j^d f(n) = \sum_{k=-\infty}^{\infty} \tilde{h}(2n-k) \cdot A_{j+1}^d f(k).$$

The proof of this statement is given in the appendix.

5.2. Dyadic Wavelet Representation

In this section it is explained how to extract the difference of information between the approximations at the resolutions 2^{j+1} and 2^{j}.
Let O_j the *orthogonal complement* of V_j in V_{j+1}:

$O_j \oplus V_j = V_{j+1}$.

The following theorem shows that we can define an orthonormal basis of O_j by scaling and translating a function $y(x)$, which is called orthogonal wavelet.

Theorem 2. Let V_j be a multiresolution vector space sequence, $\phi(x)$ the scaling function and *H* the corresponding conjugate filter. If $y(x)$ is the function whose Fourier transform is given by:
$\Psi(\omega) = G\left(\frac{\omega}{2}\right)\Phi\left(\frac{\omega}{2}\right)$, with $G^{\bullet}(w) = e^{jw}H(w+p)$, then $\left(\sqrt{2^{-j}}\psi_j\left(x-2^{-j}n\right)\right)_{n\in Z}$ is an orthonormal basis of O_j.

The time and frequency representation of $y(x)$ is given in figure 5.2.1.

The scheme for constructing the orthonormal basis of O_j goes as follows:

- given $f(x)$, *H* can be derived.
- from perfect reconstruction conditions (i.e. constructing $A_{j+1}^{d}f$ from its projections in V_j and O_j), we find $G^{\bullet}(w) = e^{jw}H(w+p)$.
- from $\Psi(\omega) = G\left(\frac{\omega}{2}\right)\Phi\left(\frac{\omega}{2}\right)$, we synthesize the wavelet $y(x)$.

We compute the orthogonal projection $P_{O_j}f$ on the vector space O_j, decomposing the signal on the orthonormal basis given by theorem 2:

$$P_{O_j}f(x) = 2^{-j}\sum_{n=-\infty}^{\infty}\left\langle f(u), y_j\left(u-2^{-j}n\right)\right\rangle y_j\left(x-2^{-j}n\right)$$

The *discrete detail* of $f(x)$ at the resolution 2^{j} is the set of the inner products:

$$D_j f(n) = \left(\left\langle f(u), y_j\left(u-2^{-j}n\right)\right\rangle\right)_{n\in Z}$$

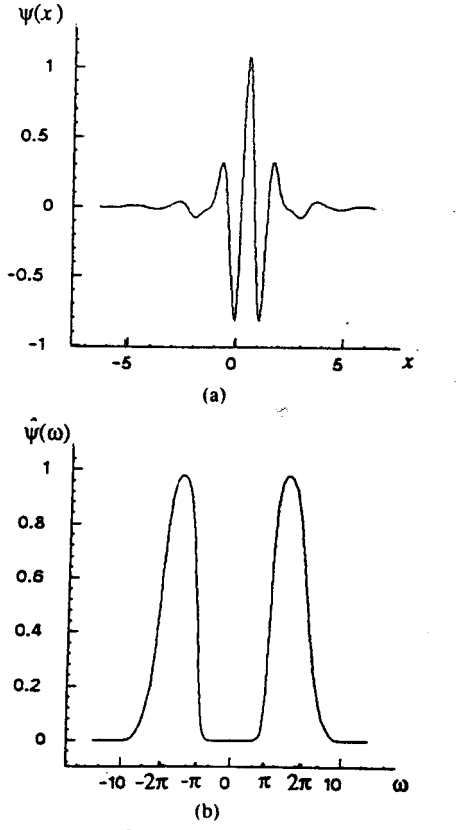

Figure 5.2.1. (a) Example of a wavelet function $y(x)$ *(associated with the scaling function given in figure 5.1.1. (b) Modulus of the Fourier transform* $\Psi(w)$*. A wavelet function is a band-pass filter.*

It can be shown that the discrete filter given by $g(n) = \langle y_{-1}(u), y(u-n) \rangle \; \forall n \in Z,$ has the transfer function $G(\omega)$ defined in theorem 2. If $\tilde{G}(\omega)$ is the symmetric filter given by $\tilde{g}(n) = g(-n)$, then $D_j f$ is computed convolving $A^d_{j+1} f$ with $\tilde{G}$ and retaining every other sample of the output:

$$D_j f(n) = \sum_{k=-\infty}^{\infty} \tilde{g}(2n-k) \cdot A^d_{j+1} f(k).$$

The impulse response of the filter *G* is related to the impulse response of the filter *H* by:

$g(n) = (-1)^{1-n} h(1-n)$ (this can be proven by starting from $G^{\bullet}(w) = e^{jw} H(w+p)$).

The *H* filter is a low pass filter while the *G* filter is a high pass filter. The time and frequency representation of *H* is given in figure 5.2.2.

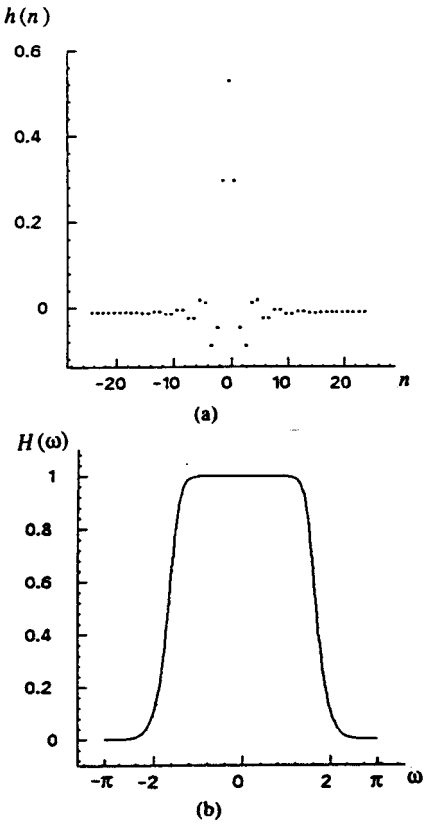

Figure 5.2.2. (a) Impulse response of the filter H associated to the scaling function shown in figure 5.1.1. (b) Transfer function $H(w)$.

The wavelet representation of the signal can be computed using a pyramidal algorithm.
The block diagram for the calculation of both the discrete approximation and discrete detail is given in the figure below.

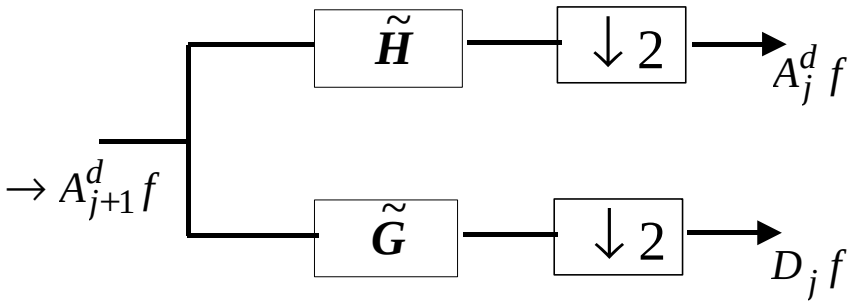

Figure 5.2.3. Decomposition of a discrete approximation $A_{2^{j+1}}^d f$ *into a approximation at a coarser resolution* $A_{2^j}^d f$ *and the detail signal* $D_{2^j} f$. *By repeating in cascade this algorithm for* $-1 \geq j \geq -J$, *we compute the wavelet representation on J levels of the original signal* $A_0^d f$.

After the multiresolution decomposition on *J* levels *(J>0)*, we obtain a set of *J+1* signals called an *orthogonal wavelet representation* of the original signal *f*:

$$\left(A_{-J}^d f,\ \left(D_j f\right)_{-J \leq j \leq -1} \right)$$

The continuous approximation $A_j f$ and the wavelet representation of a signal at several resolutions are given in figure 5.2.4.

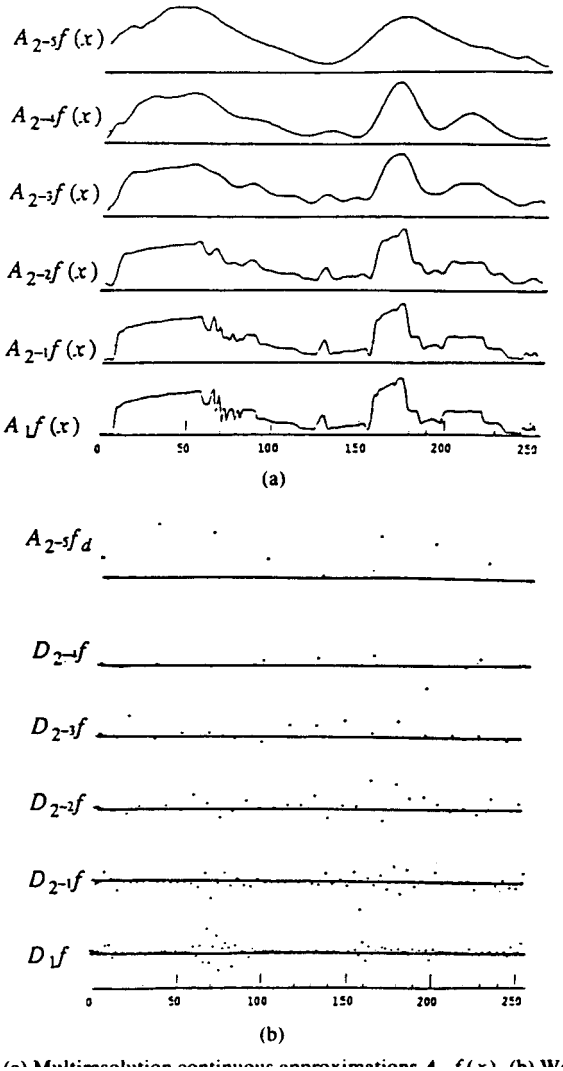

Figure 5.2.4. (a) Multiresolution continuous approximations $A_j f$ (or $A_{2^j} f$ in the figure). (b) Wavelet representation of the signal $A_1 f$. The detail samples have a high amplitude when the approximations $A_{2^j} f$ and $A_{2^{j+1}} f$ shown in (a) are locally different.

5.3. Signal Reconstruction from a Wavelet Representation

The signal can be recovered from a wavelet representation with a pyramidal algorithm. The discrete approximation $A^d_{j+1} f$ is reconstructed from $A^d_j f$ (the approximation of the signal at the coarser resolution 2^j), and the detail signal $D_j f$:

$$A^d_{j+1} f(n) = 2 \sum_{k=-\infty}^{\infty} h(n-2k) \cdot A^d_j f(k) + 2 \sum_{k=-\infty}^{\infty} g(n-2k) \cdot D_j f(k).$$

The block diagram of the signal reconstruction (or signal synthesis) from its wavelet representation is given in figure 5.3.1.

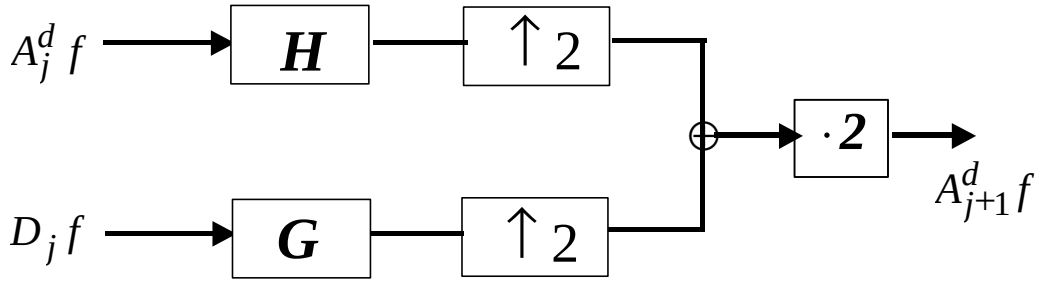

Figure 5.3.1. Reconstruction of a discrete approximation $A_{2^{j+1}}^d f$ *from an approximation at a coarser resolution* $A_{2^j}^d f$ *and the signal detail* $D_{2^j} f$ *. By repeating in cascade this algorithm for* $-J \le j \le -1$*, we reconstruct* $A_0^d f$ *from its wavelet representation.*

5.4. Orthogonal Wavelet Representation of Images

A multiresolution decomposition of an image on *J* levels (*J>0*), results into a set of $3xJ+1$ images called the orthogonal wavelet representation of the original image *f* :

$(A_{-J} f,\ WX_j f,\ WY_j f,\ WXY_j f)_{-J \le j \le -1}$.

The decomposition scheme for 2D analysis is depicted in figure 5.4.1 and consists in successively applying the one-dimensional DWT on the rows and on the columns of the image matrix. We first convolve the rows of $A_{j+1} f$ with a one-dimensional filter, retain every other sample, convolve the columns of the resulting signals with another one-dimensional filter and retain every other sample.

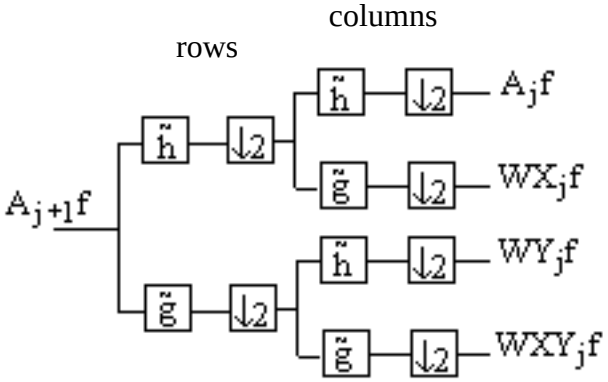

Figure 5.4.1. Wavelet subband analysis of images.

The one-dimensional reconstruction algorithm can be extended in two dimensions. The 2D multiresolution synthesis scheme is illustrated by the block diagram in figure 5.4.2. At each step, the image $A_{j+1}^d f$ is reconstructed from $A_j^d f$, $WX_j f$, $WY_j f$ and $WXY_j f$. Between each column of the images $A_j^d f$, $WX_j f$, $WY_j f$ and $WXY_j f$, we add a column of zeros, convolve the rows with a one dimensional filter, add a row of zeros between each row of the resulting image, and convolve the columns with another one-dimensional filter. The filters used in reconstruction are the quadrature mirror filters *H* and *G* described in section 5.2.

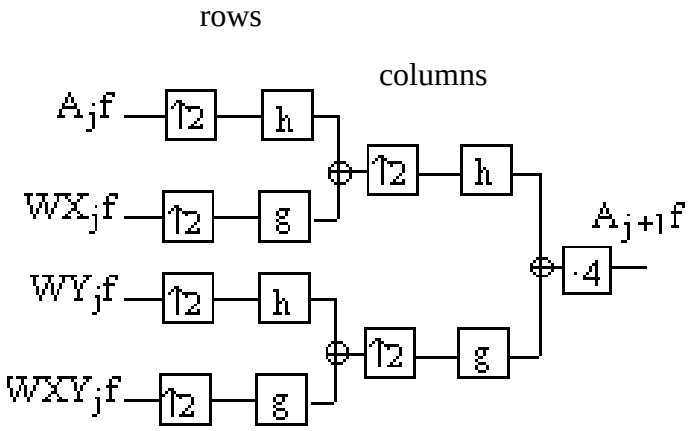

Figure 5.4.2. Wavelet subband synthesis of images.

The algorithms of analysis and synthesis are applied *J*-times successively for a *J*-level decomposition-reconstruction scheme.

6. Wavelet Bases & Filter Banks

Our focus in this chapter will be directed to series expansions of discrete time sequences and to its links with perfect reconstruction filter banks. As in the previous chapters, the theory presented in this chapter will be formalized for one-dimensional signals, details being provided for cases in which the extension to the two dimensional case is not straightforward.
The reasons for expanding signals are related to signal analysis, approximation and compression, as well as algorithms and implementations. Thus, given an arbitrary sequence $x[n]$, we would like to write it as:

$$x[n] = \sum_{k \in Z} \langle j_k, x \rangle j_k[n], \quad n \in Z .$$

Therefore, we would like to construct orthonormal sets of basis functions $\{j_k[n]\}$, which are complete in the space of square-summable sequences $l^2(Z)$. The discrete-time Fourier series is an example of such an orthogonal series expansion, but it has a number of shortcomings. Discrete-time bases better suited for signal processing tasks will try to satisfy two conflicting requirements, namely to achieve good frequency resolution while preserving good time locality as well. Additionally, for both practical and computational reasons, the set of basis functions $\{j_k[n]\}$ has to be structured. Typically, the infinite set of basis functions $\{j_k[n]\}$ is obtained from a finite number of prototype functions and their shifted versions in time, This leads to discrete-time *filter banks* for the implementation of such structured expansions.
The structure of this chapter is as follows: section 6.1 examines two channel filter banks in detail and presents the three mathematical tools widely used to analyze them: time-domain analysis, modulation-domain analysis and polyphase domain analysis. Several issues like vanishing moments, support, moments, and regularity of a wavelet function are discussed in section 6.2. Finally, various types of wavelet bases including the Haar, Sinc, Meyer, and Battle-Lemarié wavelets and theory of biorthogonal wavelet bases are presented in detail in section 6.3.

6.1. Two-Channel Filter Banks

The aim of this section is to examine two-channel filter banks in detail and using them as an illustration to present the mathematical tools needed for analyzing filter banks in general. The main idea of this section is that perfect reconstruction filter banks implement series expansions of discrete-time signals and in order to develop this idea we start by recalling some general properties of discrete-time expansions.

Consider $x[n]$ an arbitrary square-summable sequence, or $x[n] \in l^2(Z)$. The *orthonormal expansion* of $x[n]$ is of the form:

$$x[n] = \sum_{k \in Z} \langle j_k[l], x[l] \rangle \cdot j_k[n] = \sum_{k \in Z} X[k] \cdot j_k[n],$$

where

$$X[k] = \langle j_k[l], x[l] \rangle$$

is the *transform* of $x[n]$. The basis functions $\{j_k[n]\}$ satisfy the orthonormality constraint:

$$\langle j_k[n], j_l[n] \rangle = d[k-l] .$$

An important property of orthonormal expansions is conservation of energy:

$\|x\|^2 = \|X\|^2$,
that is, the energy in the original domain is equal to the energy in the transformed domain.

Biorthogonal expansions on the other hand are given by:
$$x[n] = \sum_{k\in Z} \langle j_k[l], x[l]\rangle \cdot \tilde{j}_k[n] = \sum_{k\in Z} \tilde{X}[k]\cdot \tilde{j}_k[n] = \sum_{k\in Z} \langle \tilde{j}_k[l], x[l]\rangle \cdot j_k[n] = \sum_{k\in Z} X[k]\cdot j_k[n],$$
where
$$X[k] = \langle j_k[l], x[l]\rangle,\ \tilde{X}[k] = \langle \tilde{j}_k[l], x[l]\rangle$$
are the transform coefficients of $x[n]$ with respect to $\{j_k\}$ and $\{\tilde{j}_k\}$. The dual bases $\{j_k\}$ and $\{\tilde{j}_k\}$ satisfy the biorthogonality constraint:
$\langle j_k[n], \tilde{j}_l[n]\rangle = d[k-l]$.
Note that in this case, conservation of energy does not hold. For stability of the expansion, the transform coefficients have to satisfy:
$$\exists A, B > 0, \quad A\sum_k |X[k]|^2 \le \|x\|^2 \le B\sum_k |X[k]|^2$$
$$\exists C, D > 0, \quad C\sum_k |\tilde{X}[k]|^2 \le \|x\|^2 \le D\sum_k |\tilde{X}[k]|^2$$
In the biorthogonal case, conservation of energy can be expressed as:
$\|x\|^2 = \langle X, \tilde{X}\rangle$.
Finally, overcomplete expansions can be either orthonormal either biorthogonal expansions, but with redundant set of functions, that is, the functions $\{j_k\}$ and $\{\tilde{j}_k\}$ used in the expansions are not linearly independent.

Time-Domain Analysis

Consider figure 6.1.1, where the block diagram of a two-channel filter bank is depicted.

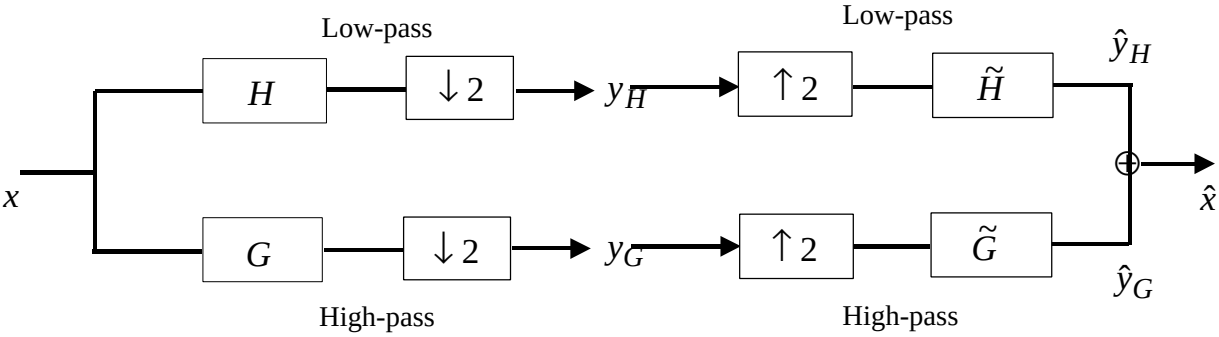

Figure 6.1.1. Two-channel filter bank with analysis filters *H*, *G* and synthesis filters $\tilde{H}, \tilde{G}$.

Our only requirement will be that such a filter bank implements a biorthogonal expansion of discrete-time signals (so not necessarily an orthonormal expansion). In filter bank literature, such a system is called a *perfect reconstruction filter bank.*
Looking at figure 6.1.1 we notice that, besides filtering, the key elements in the filter bank computation of an expansion are the downsamplers and upsamplers. These perform the sampling rate changes and the downsampler creates a periodically time-varying linear system.

Special analysis techniques are needed for such systems. We will present three ways to look at periodically time-varying linear systems, namely in time, modulation and polyphase domains. The first approach will be discussed in this section. The other two approaches are based on the *Z*-transform and aim at decomposing the periodically time-varying systems into several time-invariant subsystems.

In time domain, the output of the analysis performed with the *H* and *G* filters followed by downsampling can be expressed via an infinite matrix as follows:

$$\begin{pmatrix} \vdots \\ y_H[0] \\ y_G[0] \\ y_H[1] \\ y_G[1] \\ \vdots \end{pmatrix} = \underbrace{\begin{pmatrix} \vdots \\ X[0] \\ X[1] \\ X[2] \\ X[3] \\ \vdots \end{pmatrix}}_{\boldsymbol{X}} = T_a \cdot \underbrace{\begin{pmatrix} \vdots \\ x[0] \\ x[1] \\ x[2] \\ x[3] \\ \vdots \end{pmatrix}}_{\boldsymbol{x}},$$

$$\boldsymbol{X} = \boldsymbol{T}_{\mathrm{a}} \cdot \boldsymbol{x}$$

where $X[k]$ are the transform coefficients and represent actually the outputs of the two branches in figure 6.1.1, that is, the two *subband* outputs denoted by:

$y_H[k] = X[2k]$

$y_G[k] = X[2k+1]$.

$\boldsymbol{T}_a$ is the *analysis matrix*, it has a block Toeplitz structure and can be expressed as:

$$\boldsymbol{T}_a = \begin{pmatrix} \vdots & \vdots & \vdots & & \vdots & \vdots & \vdots \\ h[L-1] & h[L-2] & h[L-3] & \ldots & h[0] & 0 & 0 \\ g[L-1] & g[L-2] & g[L-3] & \ldots & g[0] & 0 & 0 \\ 0 & 0 & h[L-1] & \ldots & h[2] & h[1] & h[0] \\ 0 & 0 & g[L-1] & \ldots & g[2] & g[1] & g[0] \\ \vdots & \vdots & \vdots & & \vdots & \vdots & \vdots \end{pmatrix},$$

where we assume that the analysis filters *H* and *G* are finite impulse response (FIR) filters of length $L = 2K$. To make the block Toeplitz structure of $\boldsymbol{T}_a$ more explicit, we can write:

$$\boldsymbol{T}_a = \begin{pmatrix} \vdots & \vdots & \vdots & \vdots & \vdots \\ A_0 & A_1 & \ldots & A_{K-1} & 0 \\ 0 & A_0 & \ldots & A_{K-2} & A_{K-1} \\ \vdots & \vdots & \vdots & \vdots & \vdots \end{pmatrix}, \quad \text{with } A_i = \begin{pmatrix} h[2K-1-2i] & h[2K-2-2i] \\ g[2K-1-2i] & g[2K-2-2i] \end{pmatrix}.$$

The transform coefficient $X[k] = \langle j_k[l], x[l] \rangle$ is:

- in the case $k = 2k'$, $y_H[k'] = \langle h[2k'-n], x[n] \rangle$
- in the case $k = 2k'+1$, $y_G[k'] = \langle g[2k'-n], x[n] \rangle$

Therefore, the analysis basis functions are :

- $j_{2k}[n] = h[2k-n]$
- $j_{2k+1}[n] = g[2k-n]$

To resynthesize the signal we use the dual-basis, *synthesis* matrix $\boldsymbol{T}_{\mathrm{s}}$:

$\hat{\boldsymbol{x}} = \boldsymbol{T}_S \cdot \boldsymbol{X} = \boldsymbol{T}_s \cdot \boldsymbol{T}_a \cdot \boldsymbol{x}$.

Similarly to $\boldsymbol{T}_a$, $\boldsymbol{T}_{\mathrm{s}}$ can be expressed as:

$$\boldsymbol{T}_s{}^T = \begin{pmatrix} \vdots & \vdots & \vdots & & \vdots & \vdots \\ \tilde{h}[0] & \tilde{h}[1] & \tilde{h}[2] & \ldots & \tilde{h}[L'-1] & 0 & 0 \\ \tilde{g}[0] & \tilde{g}[1] & \tilde{g}[2] & \ldots & \tilde{g}[L'-1] & 0 & 0 \\ 0 & 0 & \tilde{h}[0] & \ldots & \tilde{h}[L'-3] & \tilde{h}[L'-2] & \tilde{h}[L'-1] \\ 0 & 0 & \tilde{g}[0] & \ldots & \tilde{g}[L'-3] & \tilde{g}[L'-2] & \tilde{g}[L'-1] \\ \vdots & \vdots & \vdots & & \vdots & \vdots & \vdots \end{pmatrix}$$

Assume that $\tilde{H}, \tilde{G}$ are FIR filters of length $L' = 2K'$. Then the block Toeplitz structure of $\boldsymbol{T}_s$ is more evident if we express $\boldsymbol{T}_s$ like:

$$\boldsymbol{T}_s{}^T = \begin{pmatrix} \vdots & \vdots & \vdots & \vdots & \vdots \\ S_0{}^T & S_1{}^T & \ldots & S_{K'-1}^T & 0 \\ 0 & S_0{}^T & \ldots & S_{K'-2}^T & S_{K'-1}^T \\ \vdots & \vdots & \vdots & \vdots & \vdots \end{pmatrix}, \quad \textit{with } S_i = \begin{pmatrix} \tilde{h}[2i] & \tilde{h}[2i] \\ \tilde{g}[2i+1] & \tilde{g}[2i+1] \end{pmatrix}.$$

The synthesis dual basis functions are:

- $\tilde{j}_{2k}[n] = \tilde{h}[n-2k]$
- $\tilde{j}_{2k+1}[n] = \tilde{g}[n-2k]$

The mathematical expressions for both analysis and synthesis have been written in the time domain. The following theorem will make the link between our initial requirement (i.e. the filter bank implements a biorthogonal expansion) and the perfect reconstruction condition imposed on filter banks.

Theorem (Vetterli). The perfect reconstruction condition is equivalent to the biorthogonality condition.

The biorthogonality condition stating that $\{j_k[n]\} = \{h[2k-n], g[2k-n]\}$ and $\{\tilde{j}_k[n]\} = \{\tilde{h}[n-2k], \tilde{g}[n-2k]\}$ form a dual basis is $\langle j_k[n], \tilde{j}_l[n] \rangle = d[k-l]$, and this is equivalent to:

$\hat{\boldsymbol{x}} = \boldsymbol{x} \Leftrightarrow \boldsymbol{T}_S \cdot \boldsymbol{T}_a \cdot \boldsymbol{x} = \boldsymbol{T}_a \cdot \boldsymbol{T}_S \cdot \boldsymbol{x} = \boldsymbol{x} \Leftrightarrow \boldsymbol{T}_S \cdot \boldsymbol{T}_a = \boldsymbol{T}_a \cdot \boldsymbol{T}_S = \boldsymbol{I}$.

The condition $\langle j_k[n], \tilde{j}_l[n] \rangle = d[k-l]$ translates in terms of filter responses into:

$k = 2k'; l = 2l' \Rightarrow \langle h[2k-n], \tilde{h}[n-2l] \rangle = d[k-l]$

$k = 2k'+1; l = 2l'+1 \Rightarrow \langle g[2k-n], \tilde{g}[n-2l] \rangle = d[k-l]$

$k = 2k'+1; l = 2l' \Rightarrow \langle g[2k-n], \tilde{h}[n-2l] \rangle = 0$

$k = 2k'; l = 2l'+1 \Rightarrow \langle h[2k-n], \tilde{g}[n-2l] \rangle = 0$.

Consider the two branches of figure 6.1.1 which produces y_H and y_G. Call $\boldsymbol{H}_a$ and $\boldsymbol{G}_a$ the operator corresponding to filtering by *H* and *G* followed by the downsampling by 2. Then the output y_H and y_G can be written as (*L* denotes the filter length):

$$\underbrace{\begin{pmatrix} \vdots \\ y_H[0] \\ y_H[1] \\ \vdots \end{pmatrix}}_{\boldsymbol{y}_H} = \underbrace{\begin{pmatrix} & \vdots & \vdots & \vdots & \\ \cdots & h[L-1] & h[L-2] & h[L-3] & \cdots \\ \cdots & 0 & 0 & h[L-1] & \cdots \\ & \vdots & \vdots & \vdots & \end{pmatrix}}_{\boldsymbol{H}_a} \underbrace{\begin{pmatrix} \vdots \\ x[0] \\ x[1] \\ \vdots \end{pmatrix}}_{\boldsymbol{x}}$$

$$\begin{pmatrix} \vdots \\ y_G[0] \\ y_G[1] \\ \vdots \end{pmatrix} = \begin{pmatrix} \vdots & \vdots & \vdots & & \\ \cdots & g[L-1] & g[L-2] & g[L-3] & \cdots \\ \cdots & 0 & 0 & g[L-1] & \cdots \\ & \vdots & \vdots & \vdots & \end{pmatrix} \begin{pmatrix} \vdots \\ x[0] \\ x[1] \\ \vdots \end{pmatrix}$$

In operator notation this is equivalent to:

$\boldsymbol{y}_H = \boldsymbol{H}_a \cdot \boldsymbol{x}$

$\boldsymbol{y}_G = \boldsymbol{G}_a \cdot \boldsymbol{x}$

Defining ${\boldsymbol{H}_s}^T$ and ${\boldsymbol{G}_s}^T$ similar to $\boldsymbol{H}_a$ and $\boldsymbol{G}_a$ but with $\tilde{h}[n]$ and $\tilde{g}[n]$ in reverse order (se also the definition of $\boldsymbol{T}_s$), the output of the system can now be written as:

$(\boldsymbol{H}_a \cdot \boldsymbol{H}_s + \boldsymbol{G}_a \cdot \boldsymbol{G}_s)\boldsymbol{x}$

To resynthesize the signal (i.e. the *perfect reconstruction condition*) we have to have:

$(\boldsymbol{H}_a \cdot \boldsymbol{H}_s + \boldsymbol{G}_a \cdot \boldsymbol{G}_s) = \boldsymbol{I}$

By interleaving the rows of $\boldsymbol{H}_a$ and $\boldsymbol{G}_a$, we get $\boldsymbol{T}_a$, and similarly, $\boldsymbol{T}_s$ corresponds to interleaving the columns of $\boldsymbol{H}_s$ and $\boldsymbol{G}_s$. As a result, the perfect reconstruction condition translates into

$\boldsymbol{T}_a \cdot \boldsymbol{T}_s = \boldsymbol{I}$,

which is the biorthogonality condition.

To summarize this part on time-domain analysis, let us stress once more that biorthogonal expansions of discrete-time signals, where the basis functions are obtained from two prototype functions and their even shifts (for both dual bases), is implemented using a perfect reconstruction, two-channel filter bank. In other words, perfect reconstruction is equivalent to the biorthogonality condition.

Modulation-Domain Analysis

In contrast with the approach presented in the previous section, which is interesting from a theoretical point of view, the approach presented in this section is based on the *Z*-transform, being much easier and much more connected to the practical applications.

Recall from the general theory on the *Z*-transform that downsampling by 2 a signal with the *Z*-transform $X(z)$ leads to $X'(z)$ given by:

$$X'(z) = \frac{1}{2}\left[X\left(z^{1/2}\right) + X\left(-z^{1/2}\right)\right]$$

Then, upsampling $X'(z)$ by 2 yields $X''(z) = X'\left(z^2\right)$, or:

$$X''(z) = \frac{1}{2}\left[X(z) + X(-z)\right].$$

To verify this last property directly, notice that downsampling followed by upsampling by 2 simply nulls out the odd-indexed coefficients, that is, $x''[2n] = x[2n]$ and $x''[2n+1] = 0$. Then, note that $X(-z)$ is the *Z*-transform of $(-1)^n x[n]$, therefore the property above follows immediately.

With this preamble, the *Z*-transform analysis of the filter bank given in figure 6.1.1 becomes easy. The results of the low-pass and high-pass filtering followed by a downsampling by 2 operation can be written as:

$$Y_H(z)=\frac{1}{2}\left[H\left(z^{1/2}\right)\cdot X\left(z^{1/2}\right)+H\left(-z^{1/2}\right)\cdot X\left(-z^{1/2}\right)\right]$$

$$Y_G(z)=\frac{1}{2}\left[G\left(z^{1/2}\right)\cdot X\left(z^{1/2}\right)+G\left(-z^{1/2}\right)\cdot X\left(-z^{1/2}\right)\right]$$

These two equations express the output of the *analysis module* in the filter bank as a function of the input $X(z)$. The *synthesis module* in the filter bank consists of an upsampling by 2 operation followed by low-pass and high-pass filtering, therefore:

$$\hat{Y}_H(z)=\tilde{H}(z)\cdot Y_H\left(z^2\right)$$

$$\hat{Y}_G(z)=\tilde{G}(z)\cdot Y_G\left(z^2\right)$$

Replacing the expressions for $Y_H\left(z^2\right)$ and $Y_G\left(z^2\right)$ we obtain:

$$\hat{Y}_H(z)=\frac{1}{2}\tilde{H}(z)\cdot\left[H(z)\cdot X(z)+H(-z)\cdot X(-z)\right]$$

$$\hat{Y}_G(z)=\frac{1}{2}\tilde{G}(z)\cdot\left[G(z)\cdot X(z)+G(-z)\cdot X(-z)\right]$$

Finally, the output of the filter bank is given by:

$$\hat{X}(z)=\hat{Y}_H(z)+\hat{Y}_G(z)=\frac{1}{2}\tilde{H}(z)\cdot\left[H(z)\cdot X(z)+H(-z)\cdot X(-z)\right]+$$
$$+\frac{1}{2}\tilde{G}(z)\cdot\left[G(z)\cdot X(z)+G(-z)\cdot X(-z)\right].$$

This is best written in matrix notation as:

$$\hat{X}(z)=\frac{1}{2}\begin{pmatrix}\tilde{H}(z) & \tilde{G}(z)\end{pmatrix}\cdot\underbrace{\begin{pmatrix}H(z) & H(-z)\\ G(z) & G(-z)\end{pmatrix}}_{\boldsymbol{H}_m(z)}\cdot\underbrace{\begin{pmatrix}X(z)\\ X(-z)\end{pmatrix}}_{\boldsymbol{X}_m(z)}$$

In the equation above, $\boldsymbol{H}_m(z)$ is the analysis modulation matrix containing the modulated versions of the analysis filters and $\boldsymbol{X}_m(z)$ contains the modulated versions of $X(z)$. This equation is illustrated in figure 6.1.2 where the time-varying part is in the lower channel.

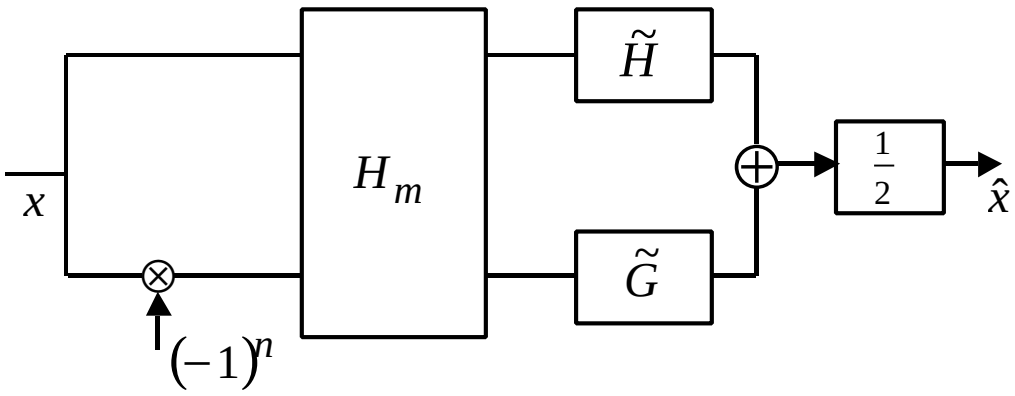

Figure 6.1.2. Modulation-domain analysis of the two-channel filter bank. The 2 *x* 2 matrix $\boldsymbol{H}_m(z)$ contains the *Z*-transform of the filters and their modulated versions.

If the channel signals $Y_H(z)$ and $Y_G(z)$ are desired, then they can be expressed in matrix notation as:

$$\begin{pmatrix} Y_H(z) \\ Y_G(z) \end{pmatrix} = \frac{1}{2}\begin{pmatrix} H\left(z^{1/2}\right) & H\left(-z^{1/2}\right) \\ G\left(z^{1/2}\right) & G\left(-z^{1/2}\right) \end{pmatrix} \cdot \begin{pmatrix} X\left(z^{1/2}\right) \\ X\left(-z^{1/2}\right) \end{pmatrix},$$

or by calling $\boldsymbol{Y}(z) = \begin{pmatrix} Y_H(z) \\ Y_G(z) \end{pmatrix}$, one obtains $\boldsymbol{Y}(z) = \boldsymbol{H}_m\left(z^{1/2}\right) \cdot \boldsymbol{X}_m\left(z^{1/2}\right)$.

The perfect reconstruction condition requires that $\hat{\boldsymbol{X}}(z) = \boldsymbol{X}(z)$. This is equivalent to:

$$\begin{cases} \tilde{H}(z) \cdot H(z) + \tilde{G}(z) \cdot G(z) = 2 \\ \tilde{H}(z) \cdot H(-z) + \tilde{G}(z) \cdot G(-z) = 0 \end{cases}$$

These two conditions can be expressed in matrix notation:

$$\left(\tilde{H}(z) \quad \tilde{G}(z)\right) \cdot \boldsymbol{H}_m(z) = (2 \quad 0)$$

We can solve now for $\left(\tilde{H}(z) \quad \tilde{G}(z)\right)$ - transpose the equation above and multiply by $\left(\boldsymbol{H}_m{}^T(z)\right)^{-1}$:

$$\begin{pmatrix} \tilde{H}(z) \\ \tilde{G}(z) \end{pmatrix} = \frac{2}{\det(H_m(z))}\begin{pmatrix} G(-z) \\ -H(-z) \end{pmatrix}$$

Define $P(z)$ as:

$$P(z) = \tilde{H}(z) \cdot H(z) = \frac{2}{\det(H_m(z))} H(z) \cdot G(-z)$$

Observe that $\det(H_m(z)) = -\det(H_m(-z))$; one can calculate then the term $\tilde{G}(z) \cdot G(z)$:

$$\tilde{G}(z) \cdot G(z) = \frac{-2}{\det(H_m(z))} H(-z) \cdot G(z) = P(-z),$$

It results that the perfect reconstruction condition can be expressed as:

$P(z) + P(-z) = 2$.

Following the definition of $P(z)$, this condition is equivalent to:

$H(z) \cdot \tilde{H}(z) + H(-z) \cdot \tilde{H}(-z) = 2$.

Using the modulation property, in time domain this is equivalent to:

$$\sum_k \tilde{h}[k] \cdot h[n-k] + (-1)^n \sum_k \tilde{h}[k] \cdot h[n-k] = 2 \Rightarrow \sum_k \tilde{h}[k] \cdot h[2n-k] = d[n] \Rightarrow$$

$$\left.\begin{array}{l} \left\langle \tilde{h}[k], h[2n-k] \right\rangle = d[n] \\ \tilde{j}_{2k}[n] = \tilde{h}[n-2k] \\ j_{2k}[n] = h[2k-n] \end{array}\right\} \Rightarrow \left\langle \tilde{j}_0[k], j_{2n}[k] \right\rangle = d[n]$$

Similarly one can obtain the other biorthogonality relations:

$\left\langle \tilde{j}_1[k], j_{2n+1}[k] \right\rangle = d[n]$

$\left\langle \tilde{j}_0[k], j_{2n+1}[k] \right\rangle = 0$

$\left\langle \tilde{j}_1[k], j_{2n}[k] \right\rangle = 0$

These conditions where obtained for $\tilde{j}_0$ and $\tilde{j}_1$, but they hold also for $\tilde{j}_{2l}$ and $\tilde{j}_{2l+1}$.

This shows once again that perfect reconstruction implies the biorthogonality condition. The converse can be shown as well, demonstrating the equivalence of the two conditions.

Polyphase-Domain Analysis

Although a very natural representation, modulation domain analysis suffers from a drawback: it is redundant. Note how in $\boldsymbol{H}_m(z)$ every filter coefficient appears twice, since both filters $H(z), G(z)$ and its modulated version $H(-z), G(-z)$ are present. A more compact way of analyzing filter banks uses the polyphase-domain analysis, which will be introduced in this section.

Definition: A *N*-size polyphase transform of a sequence $x[n]$ is a vector of sequences $(x_0[n], x_1[n], ..., x_{N-1}[n])^T$, where $x_i[n] = x[nN + i]$.

Example: $N = 2 \Rightarrow$ odd and even samples: $x_0[n] = x[2n]; \quad x_1[n] = x[2n+1];$

The result is that $X(z)$ is written as a sum of shifted and upsampled polyphase components:

$$X(z) = \sum_{i=0}^{N-1} z^{-i} X_i\left(z^N\right), \quad \text{where } X_i(z) = \sum_{i=-\infty}^{\infty} x[nN+i] z^{-n}$$

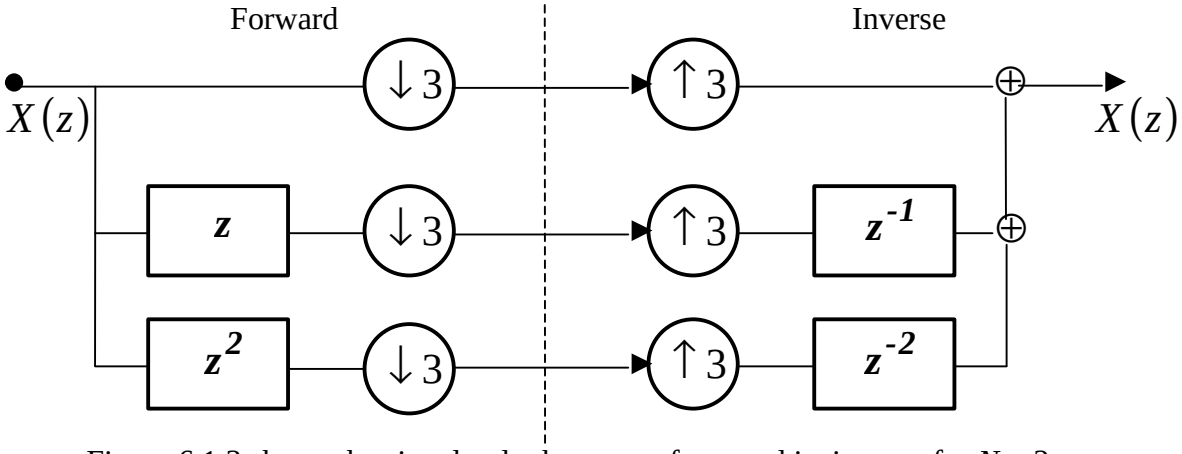

Figure 6.1.3 shows the signal polyphase transform and its inverse for $N = 3$.

Now, in order to perform a polyphase-domain analysis of the filter bank in figure 6.1.1, we need to express the output of the filtering and downsampling operations in terms of the polyphase components. For convenience, we introduce matrix notations to express the two channel signals $Y_H(z)$ and $Y_G(z)$:

$$\underbrace{\begin{pmatrix} Y_H(z) \\ Y_G(z) \end{pmatrix}}_{\boldsymbol{Y}(z)} = \underbrace{\begin{pmatrix} H_0(z) & H_1(z) \\ G_0(z) & G_1(z) \end{pmatrix}}_{\boldsymbol{A}_p(z)} \cdot \underbrace{\begin{pmatrix} X_0(z) \\ X_1(z) \end{pmatrix}}_{\boldsymbol{X}_p(z)},$$

The column vector $\boldsymbol{Y}(z)$ contains the two channel signals $Y_H(z)$ and $Y_G(z)$, while $\boldsymbol{X}_p(z)$ contains the polyphase components of the input signal, that is:

$$X(z) = X_0\left(z^2\right) + z^{-1} X_1\left(z^2\right).$$

In the equation above the matrix $\boldsymbol{A}_p(z)$ (which is called the *analysis polyphase matrix*) contains $H_0(z), H_1(z)$ and $G_0(z), G_1(z)$ which are the polyphase components of $H(z)$ and $G(z)$ respectively. We need to express the output of filtering with $H(z)$ and $G(z)$ followed by downsampling in terms of the polyphase components of the input signal. That is, we need the 0^{th} polyphase components of $H(z)X(z)$ and $G(z)X(z)$ respectively. This is easiest if we define the polyphase decomposition of the analysis filters to have the reverse phase of the one used for the signal, that is:

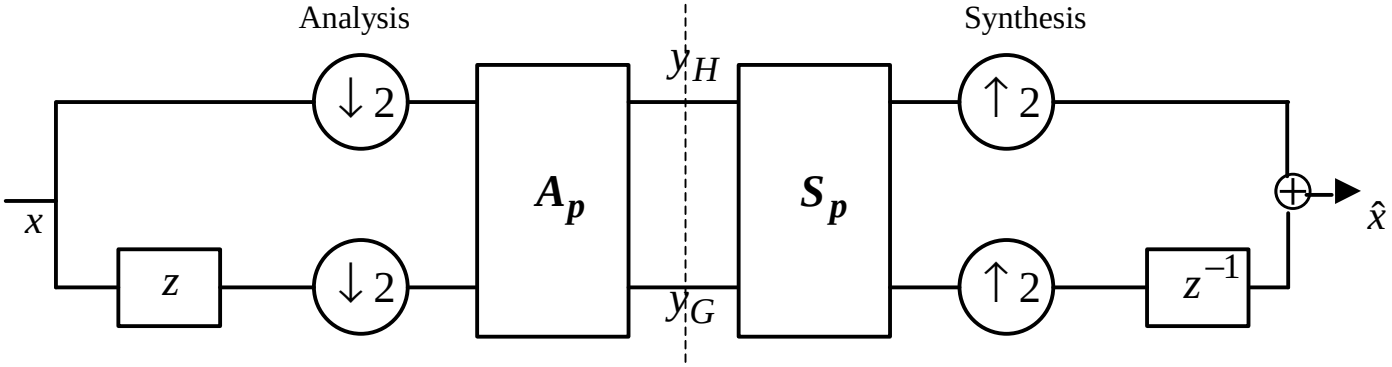

Figure 6.1.4. Polyphase domain analysis. Left part illustrates the analysis module of the filter bank in figure 6.1.1 represented in the polyphase domain, while the right part illustrates the synthesis module in the polyphase domain.

$$\begin{cases} H(z) = H_0\left(z^2\right) + zH_1\left(z^2\right) \\ G(z) = G_0\left(z^2\right) + zG_1\left(z^2\right) \end{cases}.$$

Having made these notations, the forward polyphase analysis of the filter bank in figure 6.1.1 is written as:

$$\boldsymbol{Y}(z) = \boldsymbol{A}_p(z) \cdot \boldsymbol{X}_p(z)$$

It is instructive to give a block diagram of this equation, as shown in figure 6.1.4.

First, the input signal $X(z)$ is decomposed into its polyphase components X_0 and X_1 using a forward polyphase transform. Then, a two-input/two-output system containing $\boldsymbol{A}_p(z)$ as transfer function matrix leads to the output $Y_H(z)$ and $Y_G(z)$.

The synthesis module of the filter bank in figure 6.1.1 can be analyzed in a similar fashion. It can be implemented with an inverse polyphase transform preceded by a two-input/two-output *synthesis polyphase matrix* defined by:

$$\boldsymbol{S}_p(z) = \begin{pmatrix} \tilde{H}_0(z) & \tilde{G}_0(z) \\ \tilde{H}_1(z) & \tilde{G}_1(z) \end{pmatrix},$$

where

$$\begin{cases} \tilde{H}(z) = \tilde{H}_0\left(z^2\right) + z^{-1}\tilde{H}_1\left(z^2\right) \\ \tilde{G}(z) = \tilde{G}_0\left(z^2\right) + z^{-1}\tilde{G}_1\left(z^2\right) \end{cases}.$$

Note that the synthesis polyphase components are defined such as those of the signal, or in reverse order of those of the analysis filters. The output signal $\hat{X}(z)$ is synthesized from the input signals $Y_H(z)$ and $Y_G(z)$ as:

$$\hat{X}(z) = \begin{pmatrix} 1 & z^{-1} \end{pmatrix} \cdot \underbrace{\begin{pmatrix} \tilde{H}_0\left(z^2\right) & \tilde{G}_0\left(z^2\right) \\ \tilde{H}_1\left(z^2\right) & \tilde{G}_1\left(z^2\right) \end{pmatrix}}_{\boldsymbol{S}_p\left(z^2\right)} \cdot \underbrace{\begin{pmatrix} Y_H\left(z^2\right) \\ Y_G\left(z^2\right) \end{pmatrix}}_{\boldsymbol{Y}\left(z^2\right)},$$

This equation reflects that the channel signals are first upsampled by 2 – leading to $Y_H\left(z^2\right)$ and $Y_G\left(z^2\right)$ – and then filtered by filters $\tilde{H}(z), \tilde{G}(z)$. Note that the product $\boldsymbol{S}_p\left(z^2\right) \cdot \boldsymbol{Y}\left(z^2\right)$ is in z^2 and can thus be implemented before the upsampler by 2 (replacing z^2 by z) as shown in figure 6.1.4.

Note the duality between the analysis and synthesis filter banks. The former uses a forward, the latter an inverse polyphase transform, while the phase reversal in the definition of the

polyphase components in analysis and synthesis comes from the fact that z and z^{-1} ar dual operators, or on the unit circle, $e^{jw} = \left(e^{-jw}\right)^*$.

Obviously, the transfer function between the forward and inverse polyphase transforms defines the analysis/synthesis filter bank. This *transfer polyphase matrix* is given by:

$$\boldsymbol{T}_p(z) = \boldsymbol{S}_p(z) \cdot \boldsymbol{A}_p(z)$$

The input-output relationship is given by:

$$\hat{X}(z) = \begin{pmatrix} 1 & z^{-1} \end{pmatrix} \cdot \boldsymbol{S}_p\left(z^2\right) \cdot \boldsymbol{A}_p\left(z^2\right) \cdot \boldsymbol{X}_p\left(z^2\right) = \begin{pmatrix} 1 & z^{-1} \end{pmatrix} \cdot \boldsymbol{T}_p\left(z^2\right) \cdot \boldsymbol{X}_p\left(z^2\right)$$

Obviously, if $\boldsymbol{T}_p(z) = \boldsymbol{I}$, we have:

$$\hat{X}(z) = \begin{pmatrix} 1 & z^{-1} \end{pmatrix} \cdot \boldsymbol{X}_p\left(z^2\right) = \begin{pmatrix} 1 & z^{-1} \end{pmatrix} \cdot \begin{pmatrix} X_0\left(z^2\right) \\ X_1\left(z^2\right) \end{pmatrix} = X(z),$$

that is, the analysis/synthesis filter bank achieves perfect reconstruction with no delay.

6.2. Choosing a wavelet

Most applications (analysis, compression, noise-removal, etc.) exploit the ability of wavelet bases to efficiently approximate particular classes of functions with few non-zero coefficients. A function *f* has few *non-zero* coefficients if most of the fine-scale wavelet coefficients are small (close to zero). The design of y must be optimized to *produce* a maximum number of coefficients $\left\langle f, y_{j,n} \right\rangle$ that are close to zero.

This depends mostly on the regularity of *f*, the number of vanishing moments of y and the size of its support. In this context, in this section one discusses several properties of the wavelet y, and, in order to construct an appropriate wavelet from a conjugate filter $h[n]$ we relate these properties to conditions on $H(w)$.

Vanishing Moments

The wavelet y has *p* vanishing moments if:

$$\int_{-\infty}^{\infty} t^k y(t)\,dt = 0, \quad for \;\; 0 \le k < p$$

Theorem (Vanishing Moments)

- Let y be a wavelet that generates an orthogonal basis. If $\Psi(w)$ is *p* times continuously differentiable at $w = 0$, then the following three statements are equivalent:
  (1) The wavelet y has *p* vanishing moments.
  (2) $\Psi(w)$ and its first *p* - 1 derivatives are zero at $w = 0$.
  (3) $H(w)$ and its first *p* - 1 derivatives are zero at $w = \pi$.

Proof:

$$\Psi^{(k)}(w) = \frac{\partial^k}{\partial w^k}\Psi(w) = \int_{-\infty}^{\infty} (jt)^k y(t) e^{-jwt}\,dt \Rightarrow \Psi^{(k)}(0) = \int_{-\infty}^{\infty} (jt)^k y(t)\,dt \rightarrow (1) \Leftrightarrow 2$$

$$\left.\begin{aligned} &\Psi(w) = e^{-jw} H^*(w+p)\Phi(w) \\ &\Phi(w) \neq 0 \end{aligned}\right\} \xrightarrow{differentiation} (2) \Leftrightarrow (3)$$

Size of Support

If f has an isolated singularity at t_0 and if t_0 is inside the support of $y_{j,n} = 2^{-j/2} y\left(2^{-j} t - n\right)$, then $\left\langle f, y_{j,n} \right\rangle$ may have a large amplitude. If y has a compact support of size K, then at each scale 2^j there are K wavelets $y_{j,n}$ whose support includes t_0.

To minimize the number of high amplitude coefficients we must reduce the support of y. The following theorem relates the support size of h to the support of j and y.

Theorem (Compact Support)

- The scaling function j has a compact support if and only if h has a compact support and their support are equal. If the support of h and j is $[N_1, N_2]$ then the support of y is $[(N_1 - N_2 + 1)/2, (N_2 - N_1 + 1)/2]$.

If h has a finite impulse response in $[N_1, N_2]$, then y has a support of size $N_2 - N_1$ centered at 1/2. To minimize the size of support of y, we must synthesize conjugate mirror filters h with as few non-zero coefficients as possible.

Size of Support versus Vanishing Moments

The support size of a function and the number of vanishing moments are a priori independent. However, as we will see in the theorem of Tchamitchian, the constraints imposed on orthogonal wavelets imply that if y has p vanishing moments, then its support is at least of size $2p$-1. Duabechies wavelets are optimal in the sense that they have a minimum size support for a given number of vanishing moments. When choosing a particular wavelet we must face a trade-off between the number of vanishing moments and the support size. If f has few isolated singularities and is very regular between singularities, we must choose a wavelet with many vanishing moments to produce a large number of small wavelet coefficients $\left\langle f, y_{j,n} \right\rangle$. On the other hand, if the density of singularities increases, it might be better to decrease the size of the wavelet's support at the cost of reducing the number of vanishing moments. Indeed, wavelets that overlap singularities create high amplitude coefficients.

Regularity

Definition (Lipschitz)

- A function f is pointwise **Lipschitz** a, $a \geq 0$ at v, if there exists $K > 0$, and a polinomial p_v of degree $m = [a]$, such that:

  $\forall t \in R, \quad |f(t) - p_v(t)| \leq K|t - v|^a$
- A function f is ***uniformly Lipschitz*** a over an interval $[a,b]$, if it is Lipschitz a for all $v \in [a,b]$, with a constant K that is independent of v.
- The Lipschitz regularity of f at v or over $[a,b]$ is the *sup* of the a such that f is Lipschitz a.

If $0 \leq a < 1$, then $p_v(t) = f(t)$, and the Lipschitz condition becomes:

$\forall t \in R, \quad |f(t) - f(v)| \leq K|t - v|^a$

The uniform Lipschitz regularity of f over R is related to the asymptotic decay of its Fourier transform, as stated by the following theorem.

Theorem. A function f is bounded and uniformly Lipschitz a over R if:

$$\int_{-\infty}^{\infty} |F(w)| \cdot (1+|w|^{a}) dw < \infty$$

If we refer to image coding applications, the regularity of y has mostly a "cosmetic" influence on the error introduced by thresholding or quantizing the wavelet coefficients. Reconstruct a signal from its wavelet representation:

$$f = \sum_{j=-\infty}^{\infty} \sum_{n=-\infty}^{\infty} \langle f, y_{j,n} \rangle y_{j,n}$$

An error e added to a coefficient $\langle f, y_{j,n} \rangle$ will add the wavelet component $e\, y_{j,n}$ to the reconstructed signal. If y is smooth, then $e\, y_{j,n}$ is a smooth error. For image coding applications, a smooth error is less visible than an irregular error, even though they have the same energy. Better quality images are obtained with wavelets that are continuously differentiable than with the discontinuous Haar wavelets. The following theorem (of Tchamitchian) relates the uniform Lipschitz regularity of j and y to the number of zeros of $H(w)$ at $w = p$.

Theorem (Tchamitchian)

- Let $H(w)$ be a conjugate mirror filter with p zeroes at p and perform the factorization:
  $$H(w) = \sqrt{2} \left(\frac{1+e^{jw}}{2} \right)^{p} L(w)$$
- If $\sup_{w \in R} |L(w)| = B$, then j and y are uniformly Lipschitz a for
  $a < a_0 = p - \log_2 B - 1$

This theorem proves that if $B < 2^{p-1}$, then $a_0 > 0$, therefore j and y are uniformly continuous. If for any m we have $B < 2^{p-1-m}$, then $a_0 > m$, therefore j and y are m times continuously differentiable. This theorem shows that the number of zeros of $H(w)$ at p is equal to the number of vanishing moments of y . However, there is no guarantee that increasing p will improve the wavelet regularity, since B might increase as well. However, for important families of conjugate mirror filters such as splines or Daubechies filters, p increases much faster than B, and as a result, the wavelet regularity increases with the number of vanishing moments. It is important to emphasize that the number of vanishing moments and the regularity are related, but it is the number of vanishing moments and not the regularity that affects the amplitude of wavelet coefficients at fine scales.

6.3. Wavelet Bases

In this section, different classes of wavelets, including wavelets constructed with Fourier techniques (Haar, Sinc, Meyer and Battle-Lemarié Wavelets), the Daubechies compactly supported wavelets, biorthogonal wavelet bases, and finally, compactly supported biorthogonal wavelets will be discussed.

6.3.1. Wavelets Constructed with Fourier Techniques

1. The simplest example of a wavelet is the *Haar* function, with the scaling function given by $j(t) = \mathbf{1}_{[0,1]}$, which yields:

$$h[n] = \begin{cases} 1/\sqrt{2}, & n = 0,1 \\ 0, & otherwise \end{cases}$$

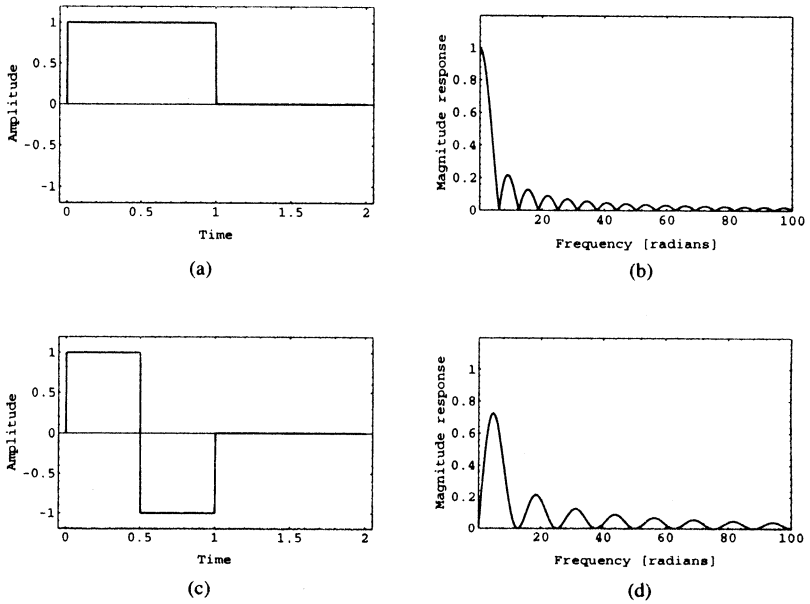

Figure 6.3.1.1. The Haar case. (a) Scaling function $f(t)$*. (b) Fourier transform magnitude* $|\Phi(w)|$*. (c) Wavelet* $-y(t)$*. (d) Fourier transform magnitude* $|\Psi(w)|$*.*

Hence:

$$\frac{1}{\sqrt{2}} y\left(\frac{t}{2}\right) = \sum_{n=-\infty}^{\infty} (-1)^{1-n} h[1-n] j(t-n) = [j(t-1) - j(t)] \Rightarrow y(t) = \begin{cases} -1, & 0 \le t < 1/2 \\ 1, & 1/2 \le t < 1 \\ 0, & otherwise \end{cases}$$

Although the Haar wavelet has the shortest support in time among all orthogonal wavelets, it is not well adapted to approximating smooth functions because it has only one vanishing moment. Moreover, the localization in frequency is not very good since decays only as $1/\omega$ when $\omega \to \infty$. The scaling function, the Fourier transform magnitude $|\Phi(w)|$, the wavelet $y(t)$ and the Fourier transform magnitude $|\Psi(w)|$ are given in figure 6.3.1.1.

2. The dual of the Haar wavelet is the *sinc* wavelet, which has finite support in frequency and decays in time as $1/t, t \to \infty$. The scaling function (see figure 6.3.1.2) is given by:

$$j(t) = \frac{\sin(p\,t)}{p\,t}, \text{ with } \Phi(w) = \begin{cases} 1, & |w| < p \\ 0, & otherwise \end{cases}.$$

The wavelet is given by:

$$y(t) = \frac{\sin(p\,(t/2 - 1/4))}{p\,(t/2 - 1/4)} \cos(3p\,(t/2 - 1/4)), \text{ with } \Psi(w) = \begin{cases} -e^{-jw/2}, & p \le |w| < 2p \\ 0, & otherwise \end{cases}$$ (see figure 6.3.1.2).

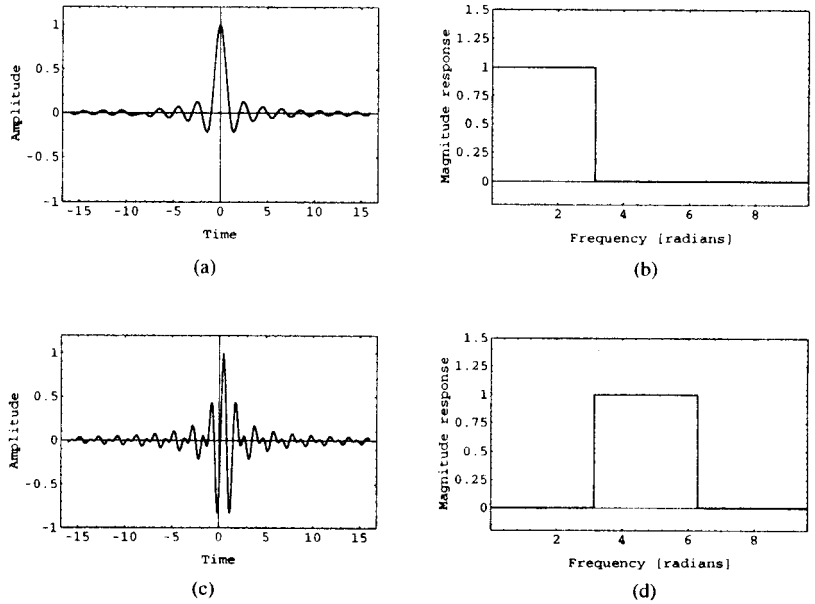

Figure 6.3.1.2. The sinc case. (a) Scaling function $f(t)$. *(b) Fourier transform magnitude* $|\Phi(w)|$. *(c) Wavelet* $y(t)$. *(d) Fourier transform magnitude* $|\Psi(w)|$.

3. Meyer Wavelets

These wavelets are frequency band-limited functions with smooth spectrum. This smoothness provides a much faster asymptotic decay in time.

Start from quadrature mirror filters $H(w)$ that satisfy

$$H(w)=\begin{cases}\sqrt{2}, & w\in[-p/3,\ \ p/3]\\ 0, & w\in[-p,\ \ -2p/3]\cup[2p/3,\ \ p]\end{cases}$$

The only degree of freedom in choosing $H(w)$ are the transition bands $[-2p/3,-p/3]\cup[p/3,2p/3]$. The quadrature condition should be satisfied:

$$|H(w)|^2+|H(w+p)|^2=1$$

In order to obtain C^n junctions at $|w|=p/3$ and $|w|=2p/3$, the n first derivatives must vanish at these abscissa. One can verify the scaling function $\Phi(w)=\prod_{p=1}^{\infty}H\left(2^{-p}w\right)$ is of the form:

$$\Phi(w)=\prod_{p=1}^{\infty}H\left(2^{-p}w\right)=\begin{cases}H(w/2), & |w|\le 4p/3\\ 0, & |w|>4p/3\end{cases}$$

The resulting wavelet is:

$$\Psi(w)=\begin{cases}0, & if\ |w|\le 2p/3\\ \frac{1}{\sqrt{2}}G\left(\frac{w}{2}\right), & if\ 2p/3\le|w|\le 4p/3\\ \frac{1}{\sqrt{2}}e^{-jw/2}H\left(\frac{w}{4}\right), & if\ 4p/3\le|w|\le 8p/3\\ 0, & if\ |w|\ge 8p/3\end{cases}$$

Since $\Psi(w)=0$ in the vicinity of $w = 0$, all its derivatives are zero at $w = 0$, which proves that y has an infinite number of vanishing moments. Also, if $H(w)$ is n-times continuously differentiable, it results that j and y are n-times continuously differentiable

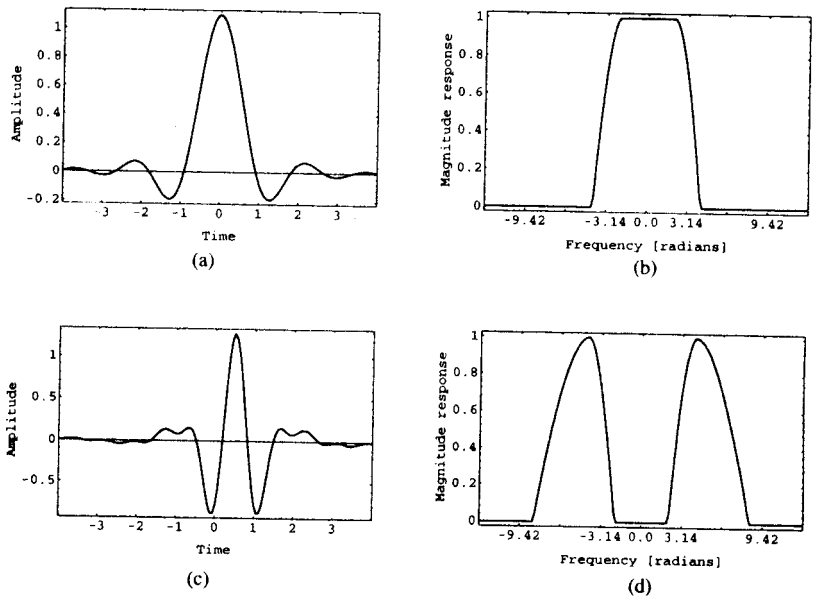

Figure 6.3.1.3. Meyer's scaling function and the wavelet. (a) Scaling function $f(t)$. *(b) Fourier transform magnitude* $|\Phi(w)|$. *(c) Wavelet* $y(t)$. *(d) Fourier transform magnitude* $|\Psi(w)|$.

Example

An example of the Meyer's scaling function and the wavelet is given in figure 6.3.1.3. In general, to satisfy the quadrature condition, one can verify that $H(w)$ may be defined in the transition band by:

$$H(w)=\cos\left[\frac{p}{2}b\left(\frac{3|w|}{p}-1\right)\right],\quad |w|\in[p/3,2p/3]$$

where $b(x)$ goes from 0 to 1 in the interval [0,1] and satisfies:

$b(x)+b(1-x)=1,\forall x\in[0,1]$.

An example due to Daubechies is:

$b(x)=x^4\left(35-84x+70x^2-20x^3\right)$,

and in this case the resulting $H(w)$ has three vanishing derivatives at $|w|=p/3,\ 2p/3$.

Generally, the time-domain scaling and wavelet functions, while of infinite support, have very fast decay; however, the associated $g(n)$ filter cannot be efficiently implemented, therefore Meyer's wavelets are more of theoretical interest.

4. Wavelets for Piecewise Polynomial Spaces (Battle - Lemmarié Wavelets)

The piecewise polynomial spaces are polynomials of degree *k* over fixed length intervals with continuous derivatives up to order *k-1* at the boundary between the intervals. Simple bases for such spaces are the *B*-splines. As an example, by starting with the *B*-spline of order 3 whose Fourier transform is given by:

$$B^3(\omega)=1-\frac{2}{3}sin^2\left(\frac{\omega}{2}\right),$$

the scaling function is defined as:

$$\Phi(\omega)=\frac{sin^2(\omega/2)}{(\omega/2)^2\sqrt{1-(2/3)sin^2(\omega/2)}}.$$

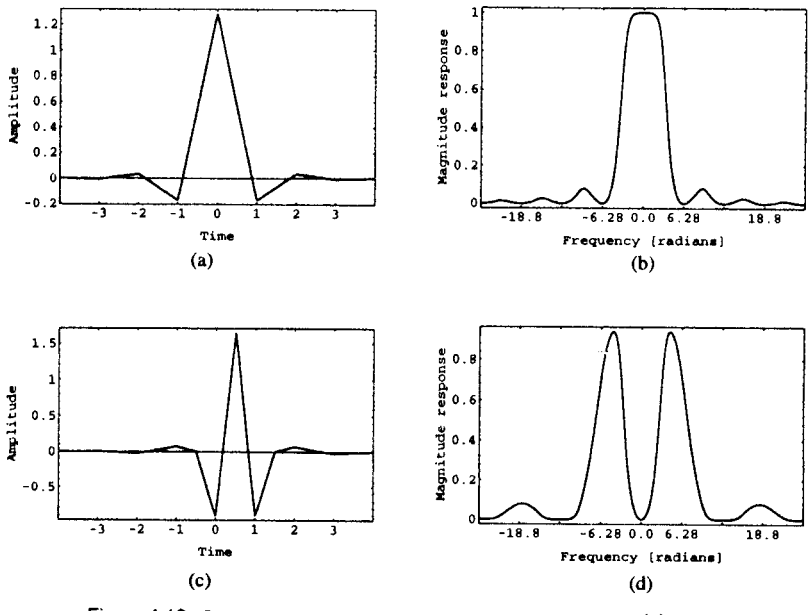

Figure 6.3.1.4. Linear spline basis. (a) Scaling function $f(t)$. *(b) Fourier transform magnitude* $|\Phi(w)|$. *(c) Wavelet* $y(t)$. *(d) Fourier transform magnitude* $|\Psi(w)|$.

In general, the scaling function for this family of wavelets is defined by:

$$\Phi(w)=\frac{e^{-jew/2}}{w^{m+1}\sqrt{S_{2m+2}(w)}}, e=\begin{cases}0 & m \text{ is odd}\\ 1 & m \text{ is even}\end{cases}, \text{ where:}$$

$$S_n(w)=\sum_{k=-\infty}^{\infty}\frac{1}{(w+2kp)^n}.$$

Starting from $S_2(w)=\sum_{k=-\infty}^{\infty}\frac{1}{(w+2kp)^2}=\frac{1}{4\sin^2(w/2)}$, by calculating the derivative of order *2m*, one can immediately derive the analytical expression for $S_{2m}(w)$, and consenquently the analytical expressions for $\Phi(w)$ and $\Psi(w)$.

As an example, the time and frequency representation for a linear spline basis (m = 1) are given in figure 6.3.1.4.

In the spline case, $\Phi(w)$, $\Psi(w)$ have infinite support but decay exponentially. Actually, polynomial spline wavelets are less regular that Meyer wavelets but have a faster time-asymptotic decay. For splines of degree *m*, $H(w)$ and its *m* derivatives are zero at $w = \pi$, and as a result y has $m + 1$ vanishing moments

If one refers to the localization properties of the scaling function, if the order of the *B*-spline is increased, the localization in time and frequency rapidly approaches the optimum since it tends to a Gaussian.

6.3.2. Daubechies Compactly supported Wavelets

Daubechies wavelets have a support of minimum size for any given number *p* of vanishing moments.

Consider that the filter $h[n]$ is a causal filter with real coefficients. This implies that $H(w)$ is a trigonometric polynomial whose Fourier series representation is given by:

$$H(w)=\sum_{n=0}^{N-1}h[n]e^{-jwn}$$

To ensure that y has p vanishing moments, the theorem of vanishing moments shows that $H(w)$ has p zeros at $w = \pi$. One can thus express $H(w)$ as:

$$H(w) = \left(\frac{1 + e^{-jw}}{2} \right)^p R(w)$$

The problem that must be solved is to design a polynomial $R(w)$ of minimum degree m such that the quadrature condition is satisfied:

$$|H(w)|^2 + |H(w + p)|^2 = 1$$

As a result, h has minimum $m + p + 1$ non-zero coefficients. The following theorem by Daubechies proves that the minimum degree of R is $m = p - 1$.

Theorem (Daubechies)

A real conjugate mirror filter h for which $H(w)$ has p zeros at $w = \pi$, has at least $2p$ non-zero coefficients. Daubechies filters have $2p$ non-zero coefficients.

The proof of this theorem is constructive and computes the Daubechies filters. This theorem shows also that $m \geq p - 1$, equality holding for the Daubechies filters. The resulting wavelet has p vanishing moments, and for $p = 1$ one obtains the Haar wavelet.

For this family of filters, j and y are highly irregular. The regularity of j and y is the same since $y(t)$ is a linear combination of the $j(2t - n)$. However, this regularity is difficult to estimate precisely. Let $B = \sup_{w \in R} |R(w)|$. The theorem of Tchamitchian proves that j and y are uniformly Lipschitz α with $a < p - \log_2 B - 1$. For Daubechies wavelets, B increases more slowly that p, therefore the regularity of these wavelets increases with p. For large p, j and y are uniformly Lipschitz α with $a \cong 0.2p$.

6.3.3. Biorthogonal Wavelet Bases

Most of the image analysis and image compression algorithms performed in the wavelet domain require the filters in the filter bank implementing the wavelet transform to be of linear phase. The main reason for this is the fact that for non-linear phase filters any operation performed in the wavelet domain is non-linearly reflected after reconstruction in the spatial domain. As an example, in image compression applications, if the filters are not of linear phase, then the quantization of the subband coefficients not only introduces amplitude distortion, but also phase distortion. However, phase distortion affects much more the quality of the reconstructed images than the amplitude distortion does, so for this kind of applications it is very important to implement the wavelet transform by using perfect reconstruction filter banks with filters of linear phase.

The problem of obtaining perfect reconstruction filter banks with linear phase is briefly discussed in this section.

If the analysis (h, g) and synthesis ($\tilde{h}$, $\tilde{g}$) filters are different, the resulting basis is non-orthogonal. The result is that different scaling and wavelet functions are used for analysis and synthesis. The relations between the analysis/synthesis scaling and wavelet functions and the analysis $H(w), G(w)$ and synthesis $\tilde{H}(w), \tilde{G}(w)$ filters are given below:

$$\Phi(2w) = H(w) \cdot \Phi(w); \quad \Psi(2w) = G(w) \cdot \Psi(w);$$

$$\tilde{\Phi}(2w) = \tilde{H}(w) \cdot \tilde{\Phi}(w); \quad \tilde{\Psi}(2w) = \tilde{G}(w) \cdot \tilde{\Psi}(w);$$

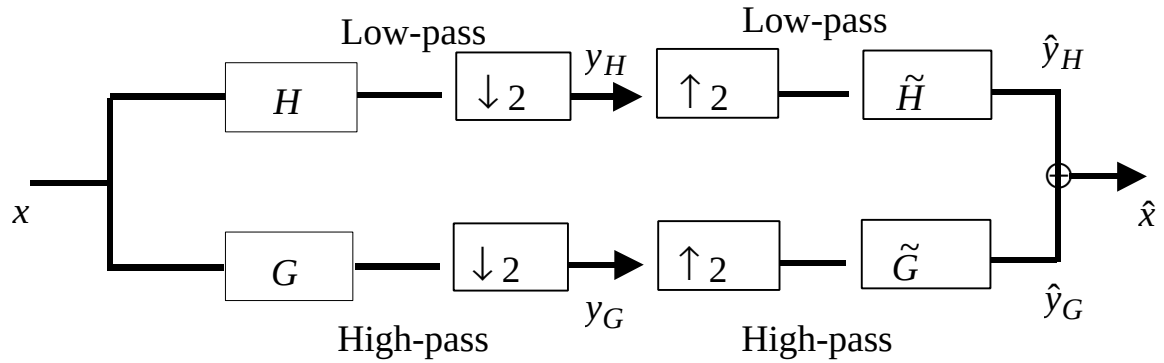

Figure 6.3.3.1. One level biorthogonal wavelet analysis/synthesis of a one-dimensional signal x

The filter bank implementing performing a one level biorthogonal wavelet analysis/synthesis of a one-dimensional signal x is shown in figure 6.3.3.1.
The perfect reconstruction condition is given by:
$H^*(w)\cdot\tilde{H}(w)+H^*(w+p)\cdot\tilde{H}(w+p)=1.$
If the filters have a finite impulse response, then:
$G(w)=e^{-jw}\tilde{H}^*(w+p),$
$\tilde{G}(w)=e^{-jw}H^*(w+p)$
The perfect reconstruction filter bank whose filters satisfy the conditions above synthesize biorthogonal wavelet bases of $L^2(R)$, and this is explained in the following.
The two wavelet families $\{y_{j,n}\}_{n\in Z}, \{\tilde{y}_{j,n}\}_{n\in Z}$ are biorthogonal Riesz bases of $L^2(R)$. Biorthogonality means that for any $n,n',j,j'\in Z^4$:
$\langle y_{j,n}, \tilde{y}_{j',n'}\rangle = d[n-n']\cdot d[j-j']$
Any $f\in L^2(R)$ has two possible decompositions in these bases, that is:

$$f=\sum_{n,j=-\infty}^{\infty}\langle f, y_{j,n}\rangle\cdot\tilde{y}_{j,n}=\sum_{n,j=-\infty}^{\infty}\langle f,\tilde{y}_{j,n}\rangle\cdot y_{j,n}$$

The Riesz stability means that there exist $A>0$ and $B>0$ such that:

$$A\|f\|^2\le\sum_{n,j=-\infty}^{\infty}\left|\langle f, y_{j,n}\rangle\right|^2\le B\|f\|^2$$

$$\frac{1}{B}\|f\|^2\le\sum_{n,j=-\infty}^{\infty}\left|\langle f,\tilde{y}_{j,n}\rangle\right|^2\le\frac{1}{A}\|f\|^2$$

Biorthogonal wavelet bases are related to multiresolution approximations. The family $\{j(t-n)\}_{n\in Z}$ is a Riesz basis of the space V_0 it generates, whereas the family $\{\tilde{j}(t-n)\}_{n\in Z}$ is a Riesz basis of another space $\tilde{V}_0$. If we let V_j and $\tilde{V}_j$ be the spaces defined by:
$f(t)\in V_j \Leftrightarrow f\left(2^j t\right)\in V_0$ and $f(t)\in\tilde{V}_j\Leftrightarrow f\left(2^j t\right)\in\tilde{V}_0,$
then one can verify that $\{V_j\}_{j\in Z}$ and $\{\tilde{V}_j\}_{j\in Z}$ are two multiresolution approximations of $L^2(R)$. It can be shown that the Riesz bases in these two vectorial spaces are the family of fnctions $j_{j,n}=\sqrt{2^j}\,j\left(2^j x-n\right)_{n\in Z}$ and $\tilde{j}_{j,n}=\sqrt{2^j}\,\tilde{j}\left(2^j x-n\right)_{n\in Z}$ respectively.

The dilated wavelets $\{y_{j,n}\}_{n\in Z}, \{\tilde{y}_{j,n}\}_{n\in Z}$ are bases of two detail spaces $O_j, \tilde{O}_j$ such that:
$V_j \oplus O_j = V_{j+1}$ and $\tilde{V}_j \oplus \tilde{O}_j = \tilde{V}_{j+1}$.
The biorthogonality of the decomposition and reconstruction wavelets implies that $O_j \perp \tilde{V}_j$ *but* $O_j \not\perp V_j$ and $\tilde{O}_j \perp V_j$ *but* $\tilde{O}_j \not\perp \tilde{V}_j$.

6.3.4. Compactly Supported Biorthogonal Wavelets

The size of support, the number of vanishing moments, the regularity, and the symmetry of biorthogonal wavelets are controlled by the choice of $h, \tilde{h}$. The following theorem relates the size of support with the number of vanishing moments and provides via a constructive approach a family of biorthogonal wavelets with a minimum size support for a given number of vanishing moments.

Theorem (Cohen, Daubechies, Feauveau)

Biorthogonal wavelets y and $\tilde{y}$ with respectively p and $\tilde{p}$ vanishing moments have a support of size at least $p + \tilde{p} - 1$. CDF biorthogonal wavelets have a minimum support of size $p + \tilde{p} - 1$.

It is possible to construct smooth biorthogonal wavelets of compact support, which are either symmetric or antisymmetric. This is impossible for orthogonal wavelets, besides the particular case of Haar basis. Symmetric or antisymmetric wavelets are synthesized with perfect reconstruction filters having a linear phase. Filters from this family - e.g. (9,7) biorthogonal filters - are often used in image compression, and for these particular filters $p = \tilde{p} = 4$.

Compactly supported biorthogonal wavelets are obtained by factorizing $H(w)$ and $\tilde{H}(w)$ as follows:

$$\begin{aligned} H(w) &= e^{-j\frac{ew}{2}}\left(\cos\frac{w}{2}\right)^{p} L(\cos w); \\ \tilde{H}(w) &= e^{-j\frac{ew}{2}}\left(\cos\frac{w}{2}\right)^{\tilde{p}} \tilde{L}(\cos w); \end{aligned} \quad \text{, with } e = \begin{cases} 0, & p, \tilde{p} \text{ even} \\ 1, & p, \tilde{p} \text{ odd} \end{cases}$$

The perfect reconstruction condition imposes:
$L(\cos w)\cdot \tilde{L}(\cos w) = P\left(\sin^2\frac{w}{2}\right)$, where the polinomial *P* must satisfy:
$(1-y)^q P(y) + y^q P(1-y) = 1, \quad \forall y \in [0,1]$
A polinomial of minimum degree satisfying this equation is:
$$P(y) = \sum_{k=0}^{q-1}\binom{q-1+k}{k}\cdot y^k$$
An example of CDF family is given by the family of biorthogonal spine wavelets. In this case,
$$H(w) = e^{-j\frac{ew}{2}}\left(\cos\frac{w}{2}\right)^{p} \text{ and } \tilde{H}(w) = e^{-j\frac{ew}{2}}\left(\cos\frac{w}{2}\right)^{\tilde{p}} \sum_{k=0}^{q-1}\binom{q-1+k}{k}\left(\sin\frac{w}{2}\right)^{2k}.$$

Appendix.

- The family of functions $\left(\sqrt{2^{-j-1}} f_{j+1}\left(x-2^{-j-1}k\right)\right)_{k\in Z}$ is an orthonormal basis of V_{j+1}.
- The family of functions $\left(\sqrt{2^{-j}} f_j\left(x-2^{-j}n\right)\right)_{n\in Z}$ is an orthonormal basis of V_j.
- $V_j \subset V_{j+1}$.

We can expand a function $\left(f_j\left(x-2^{-j}n\right)\right) \in V_j$ in the orthonormal basis of V_{j+1}:

$$f_j\left(x-2^{-j}n\right) = 2^{-j-1}\cdot \sum_{k=-\infty}^{\infty} \left\langle f_j\left(u-2^{-j}n\right), f_{j+1}\left(u-2^{-j-1}k\right)\right\rangle \cdot f_{j+1}\left(x-2^{-j-1}k\right). \quad (1)$$

$$I(k) = \left\langle f_j\left(u-2^{-j}n\right), f_{j+1}\left(u-2^{-j-1}k\right)\right\rangle = \int_{-\infty}^{\infty} f_j\left(u-2^{-j}n\right)\cdot f_{j+1}\left(u-2^{-j-1}k\right)du\,.$$

From their definition: $f_j(x) = 2^j \cdot f\left(2^j x\right)$. It follows:

$$I(k) = \int_{-\infty}^{\infty} 2^{2j+1} f\left(2^j u-n\right)\cdot f\left(2^{j+1}u-k\right)du\,.$$

Change the variable: $2^j u - n = p, \Rightarrow \begin{cases} u = 2^{-j}\left(p+n\right), \\ du = 2^{-j}\,dp \end{cases}$

It follows: $I(k) = \int_{-\infty}^{\infty} 2^{j+1} f\left(p\right)\cdot f\left(2\left(p+n\right)-k\right)dp = 2^{j+1}\cdot \int_{-\infty}^{\infty} f\left(p\right)\cdot f\left(2p-(k-2n)\right)dp\,.$

Change again: $p \to p/2$:

$$I(k) = 2^{j+1}\cdot \int_{-\infty}^{\infty} 2^{-1} f\left(2^{-1}p\right)\cdot f\left(p-(k-2n)\right)dp\,.$$

In general, $f_j(x) = 2^j \cdot f\left(2^j x\right) \Rightarrow f_{-1}(x) = 2^{-1} f\left(2^{-1}x\right)$. Therefore:

$$I(k) = 2^{j+1}\cdot \int_{-\infty}^{\infty} f_{-1}\left(p\right)\cdot f\left(p-(k-2n)\right)dp = 2^{j+1}\cdot \left\langle\ f_{-1}\left(p\right),\, f\left(p-(k-2n)\right)\ \right\rangle.$$

Go back to (1):

$$f_j\left(x-2^{-j}n\right) = \sum_{k=-\infty}^{\infty} \left\langle f_{-1}(u), f\left(u-(k-2n)\right)\right\rangle \cdot f_{j+1}\left(x-2^{-j-1}k\right). \quad (2)$$

Denote by *H* the discrete filter whose impulse response is given by:
$\forall n \in Z, \quad h\left(n\right) = \left\langle \phi_{-1}(u), \phi\left(u-n\right)\right\rangle$

That means that (2) is:

$$f_j\left(x-2^{-j}n\right) = \sum_{k=-\infty}^{\infty} h(k-2n)\cdot f_{j+1}\left(x-2^{-j-1}k\right). \quad (3)$$

Let $\tilde{H}$ be the mirror filter with the impluse response: $\tilde{h}(n) = h(-n)$. Equation (3) becomes:

$$f_j\left(x-2^{-j}n\right) = \sum_{k=-\infty}^{\infty} \tilde{h}(2n-k)\cdot f_{j+1}\left(x-2^{-j-1}k\right) \quad (4)$$

Using (4), the projection of an arbitrary function $f(x)$ on $f_j\left(x-2^{-j}n\right)$ can be written as:

$$\left\langle f(x), f_j\left(x-2^{-j}n\right)\right\rangle = \sum_{k=-\infty}^{\infty} \tilde{h}(2n-k)\cdot\left\langle f(x), f_{j+1}\left(x-2^{-j-1}k\right)\right\rangle. \quad (5)$$

The *discrete approximation* of $f(x)$ at the resolution 2^j is given by:

$$A_j^d f(n) = \left(\left\langle f(u), f_j\left(u-2^{-j}n\right)\right\rangle \right)_{n\in Z}.$$

Equation (5) can be written:

$$A_j^d f(n) = \sum_{k=-\infty}^{\infty} \tilde{h}(2n-k)\cdot A_j^d f(k) = \sum_{k=-\infty}^{\infty} \tilde{h}(k)\cdot A_j^d f(2n-k).$$

From (5) we deduce that $A_j^d f(n)$, the discrete approximation of $f(x)$ at the resolution 2^j can be computed by convolving $A_{j+1}^d f(n)$ with $\tilde{H}$ and keeping every other sample of the output. All the discrete approximations $A_j^d f$, for $j<0$, can thus be computed from $A_1^d f$ by repeating this process. This operation is called a ***pyramid transform***.

References

[1] S. Mallat. A theory for the multiresolution signal decomposition: the wavelet representation. *IEEE Transactions on Pattern Recognition and Machine Intelligence*, vol. 11, no. 7, pp. 674-693, July 1989.

[2] O. Rioul and M. Vetterli. Wavelets and signal processing. *IEEE Signal Processing Magazine*, vol. 8, no. 4, pp. 14-38, October 1991.

[3] I. Daubechies. The wavelet transform, time-frequency localization and signal analysis. *IEEE Transactions on Information Theory*, vol. 36, no. 5, pp. 961-1005, September 1990.

[4] I. Daubechies. *Ten lectures on wavelets*. SIAM, Philadelphia, PA, 1992.

[5] M. Vetterli, Jelena Kovacevic. *Wavelets and subband coding*. Prentice Hall, 1995.

[6] S. Mallat. *A wavelet tour of signal processing*, Academic Press, 1998.